

# Redshifting the Study of Cold Brown Dwarfs and Exoplanets: the Mid-Infrared Wavelength Region as an Indicator of Surface Gravity and Mass

S. K. LEGGETT <sup>1</sup> AND PASCAL TREMBLIN <sup>2</sup>

<sup>1</sup>*Gemini Observatory/NSF's NOIRLab, 670 N. A'ohoku Place, Hilo, HI 96720, USA*

<sup>2</sup>*Universite Paris-Saclay, UVSQ, CNRS, CEA, Maison de la Simulation, 91191, Gif-sur-Yvette, France*

## ABSTRACT

*JWST* is opening many avenues for exploration. For cold brown dwarfs and exoplanets, *JWST* has opened the door to the mid-infrared wavelength region, where such objects emit significant energy. For the first time, astronomers have access to mid-infrared spectroscopy for objects colder than 600 K. The first spectra appear to validate the model suite known as ATMO 2020++: atmospheres which include disequilibrium chemistry and have a non-adiabatic pressure-temperature relationship. Preliminary fits to *JWST* spectroscopy of Y dwarfs show that the slope of the energy distribution from  $\lambda \approx 4.5 \mu\text{m}$  to  $\lambda \approx 10 \mu\text{m}$  is very sensitive to gravity. We explore this phenomenon using PH<sub>3</sub>-free ATMO 2020++ models and updated *WISE* W2 – W3 colors. We find that an absolute 4.5  $\mu\text{m}$  flux measurement constrains temperature, and the ratio of the 4.5  $\mu\text{m}$  flux to the 10 – 15  $\mu\text{m}$  flux is sensitive to gravity and less sensitive to metallicity. We identify 10 T dwarfs with red W2 – W3 colors which are likely to be very low gravity, young, few-Jupiter-mass objects; one of these is the previously known COCONUTS-2b. The unusual Y dwarf WISEPA J182831.08+265037.8 is blue in W2 – W3 and we find that the 4 to 18  $\mu\text{m}$  *JWST* spectrum is well reproduced if the system is a pair of high gravity 400 K dwarfs. Recently published *JWST* colors and luminosity-based effective temperatures for late-T and Y dwarfs further corroborate the ATMO 2020++ models, demonstrating the potential for significant improvement in our understanding of cold very low-mass bodies in the solar neighborhood.

*Keywords:* Brown dwarfs — Exoplanet astronomy — Fundamental parameters of stars  
— Infrared photometry

## 1. INTRODUCTION

Wien's law of blackbody radiation states that the peak of the energy distribution will occur at wavelengths inversely proportional to temperature. Although stars and brown dwarfs (objects with a mass too low for stable hydrogen fusion e.g. Burrows & Liebert (1993); Saumon & Marley (2008); Phillips et al. (2020)) are not blackbodies, an increasing amount of energy is emitted at longer wavelengths as their effective temperature ( $T_{\text{eff}}$ ) decreases. The known T- and Y-type brown dwarfs

have  $T_{\text{eff}}$ s approximately 1200 – 500 K and 500 – 250 K respectively (e.g. Kirkpatrick et al. 2021a); Figure 1 illustrates how the bulk of the energy emission shifts from the near-infrared to the mid-infrared as late-T dwarfs cool to Y dwarfs.

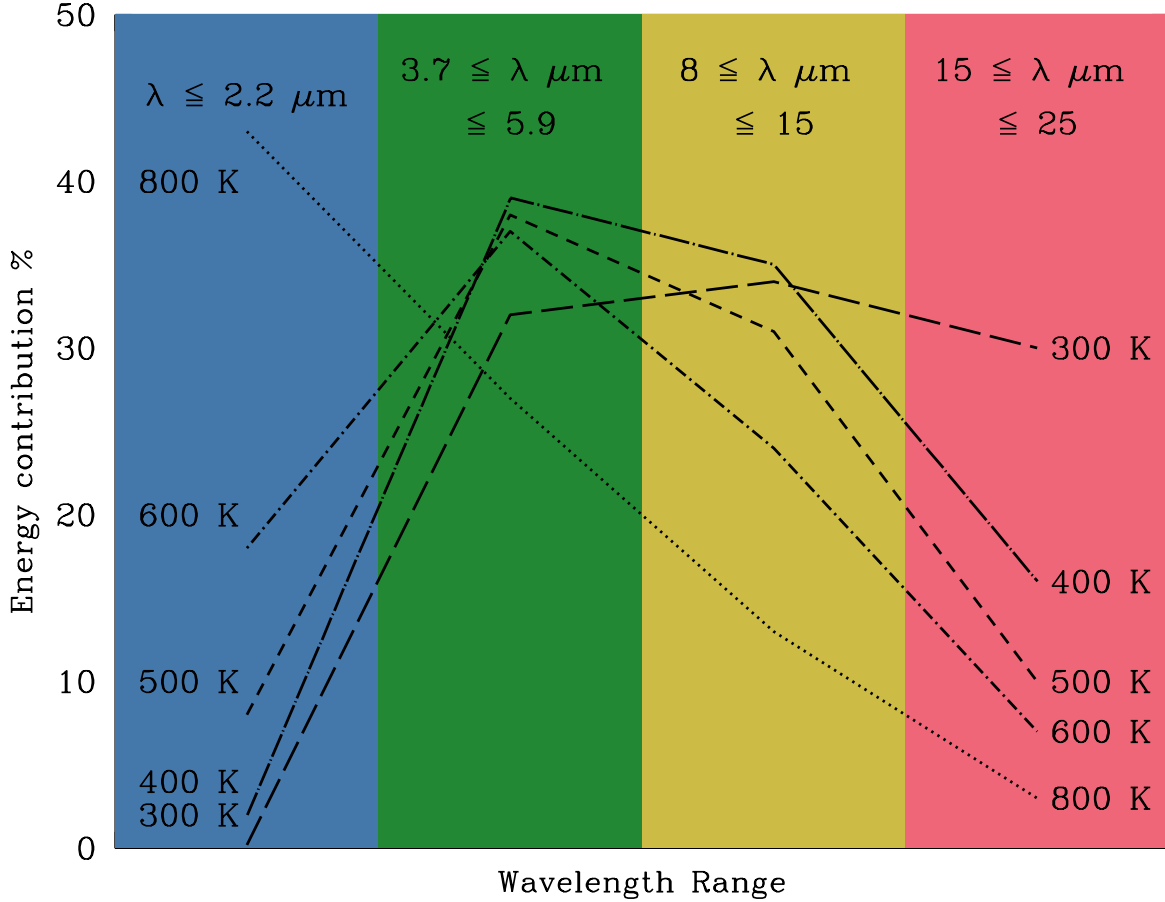


**Figure 1.** Illustration of the energy distribution shift to longer wavelengths as  $T_{\text{eff}}$  decreases, for late-T and Y dwarfs. The fractional energy contribution is estimated using ATMO 2020++ model atmospheres (Phillips et al. 2020; Leggett et al. 2021) with solar metallicity and a surface gravity  $\log g = 4.5$ . Note that approximately one-third of the total energy emerges at  $3.7 \leq \lambda \mu\text{m} \leq 5.9$ , which corresponds to the *WISE* W2, *Spitzer* [4.5], or *JWST* F444W band. For Y dwarfs, with  $T_{\text{eff}} \lesssim 500$  K, an additional third emerges at  $8 \leq \lambda \mu\text{m} \leq 15$ , which corresponds to the *WISE* W3 band.

The *Wide-field Infrared Survey Explorer* (*WISE*, Wright et al. 2010) provided vital mid-infrared imaging data, enabling discovery and characterization of very cold brown dwarfs (e.g. Cushing et al. 2011; Kirkpatrick et al. 2011; Meisner et al. 2020a; Leggett et al. 2021). A synthetic Y dwarf spectrum is shown in Figure 2 with filter profiles superimposed. The *WISE* W2 ( $4.6 \mu\text{m}$ ) and W3 ( $12 \mu\text{m}$ ) filters sample wavelength regions where significant flux is emitted (Figures 1 and 2). We note that the flux peak centered near  $\lambda = 4.5 \mu\text{m}$  lies in a window between absorption bands of  $\text{CH}_4$  at  $\lambda \sim 3 \mu\text{m}$  and  $\text{H}_2\text{O}$  at  $\lambda \sim 5 \mu\text{m}$  (e.g. Morley et al. 2014, their Figure 7), and is accessible by ground-based telescopes. The diagnostic power of this bandpass has been recognised for some time (e.g. Noll et al. 1997; Burrows et al. 2003; Leggett et al. 2007, 2010).

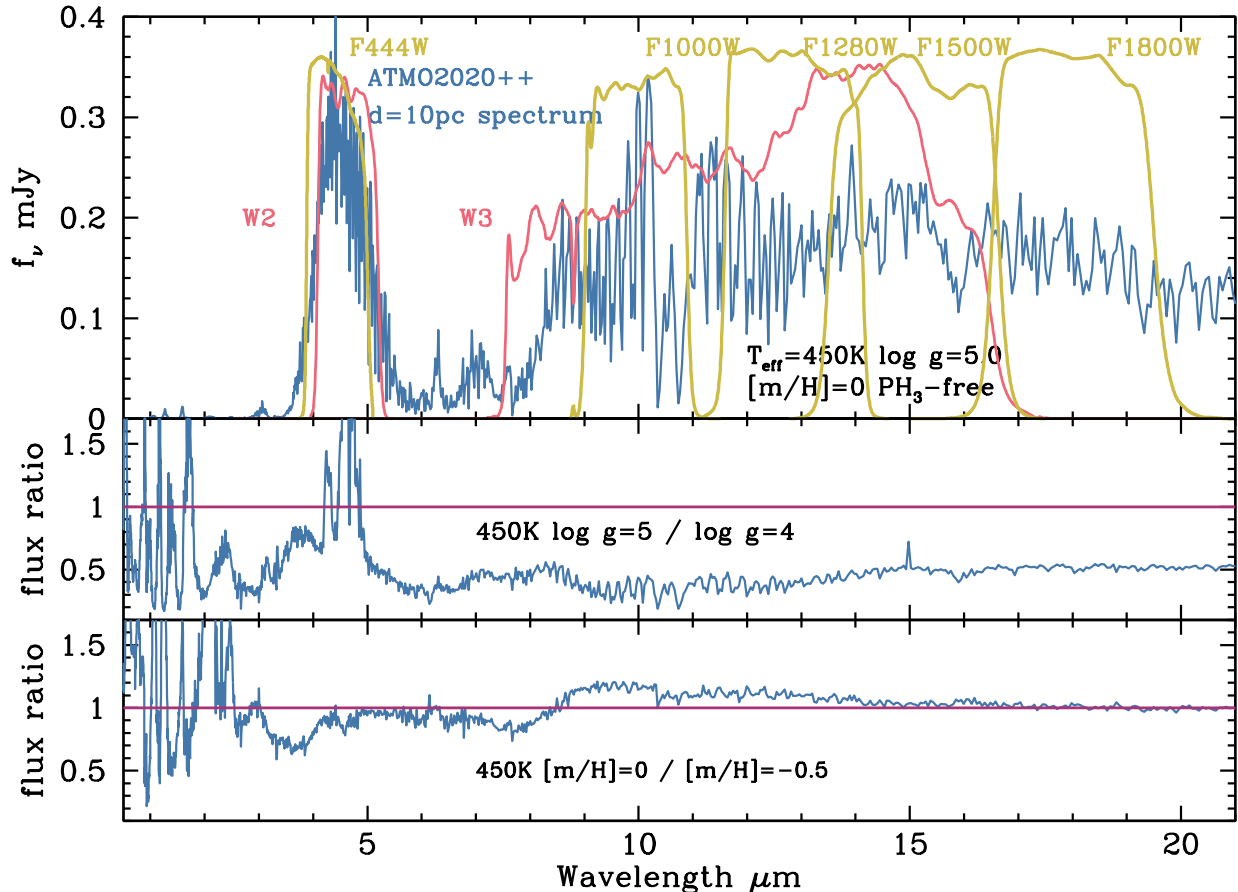


**Figure 2.** The top panel shows the synthetic spectrum for a Y dwarf at 10 pc with the atmospheric parameters given in the legend. *WISE* and *JWST* filter bandpasses are illustrated as red and yellow lines respectively. The middle and lower panels show the ratio of this spectrum divided by a spectrum where the surface gravity has been reduced, and by a spectrum where the metallicity is reduced, respectively. The total energy emitted by the lower gravity dwarf is greater because the radius is larger (Marley et al. 2021), hence the average value in the middle panel is  $< 1$ . Note that all three models have similar flux levels averaged over the  $\lambda \approx 4.5 \mu\text{m}$  flux peak, for example through an imaging filter, although the strength of the absorption features at these wavelengths (primarily due to CO and CO<sub>2</sub>) are sensitive to gravity. See Section 3 for further discussion.

The *James Webb Space Telescope* (*JWST*) is now obtaining mid-infrared spectra of Y dwarfs (Beiler et al. 2023; Barrado et al. 2023; Beiler et al. 2024). These are the first spectra of Y dwarfs at  $\lambda > 5 \mu\text{m}$  and they enable more rigorous testing of brown dwarf model atmospheres. The new data appear to validate the model suite known as ATMO 2020++: atmospheres which include disequilibrium chemistry and have a non-adiabatic pressure-temperature relationship (Tremblin et al. 2019; Phillips et al. 2020; Leggett et al. 2021; Leggett & Tremblin 2023, 2024). Leggett & Tremblin (2024) show preliminary fits of ATMO 2020++ synthetic spectra to low resolution *JWST* spectra. A striking feature is the dependency of the spectral shape on surface gravity  $g$ . In particular the relative heights of the  $\lambda \approx 4.5 \mu\text{m}$  and  $\lambda \approx 10 \mu\text{m}$  flux peaks are very different for  $\log g = 4.0$  and  $\log g = 4.5$

at  $T_{\text{eff}} = 450$  K. This observation led to the exploration of the dependency of the *WISE* W2 and W3 colors on gravity, presented here.

Section 2 describes the sample and presents updated W3 magnitudes. Section 3 presents our analysis, which includes identification of candidate low gravity (very low mass) T dwarfs, and exploration of the unusual Y dwarf WISEPA J182831.08+265037.8 as an example of a high gravity system. Section 4 applies the technique to a set of *JWST* colors, and shows that the observed colors and luminosities recently published by Beiler et al. (2024), for a sample of 22 late-T and Y dwarfs, further corroborates the ATMO 2020++ models. Section 5 gives our conclusions. The Appendix provides our photometric data compilation.

## 2. SAMPLE AND DATA

For this study we started with the photometry compilation for late-T and Y dwarfs presented in Appendix C of Leggett et al. (2021). To this sample we added the seven T dwarfs from Rothermich et al. (2024) which were not already included in the 2021 sample. Rothermich et al. (2024) identified these T dwarfs as wide companions to main sequence stars and hence they are potentially important benchmark objects: CWISE J091558.53+254713.0; CWISE J101017.43-242300.4; CWISE J104053.42-355029.7; CWISE J195956.16-644318.1; CWISE J212342.88+655615.6; CWISE J225525.22-302320.8; CWISE J233531.55+014219. We adopted the  $J, H, K, W1, W2$  (or a subset), and the parallaxes, given by Rothermich et al. (2024) for the seven dwarfs. VIKING VISTA survey  $Y$  photometry was added for CWISE J225525.22-302320.8 (Edge et al. 2013). For CWISE J233531.55+014219.6, where only a limit on  $J$  was available, we measured a magnitude from the UKIDSS LAS survey image (Lawrence et al. 2007), determining  $J = 19.53 \pm 0.20$ . AllWISE W3 was added for CWISE J104053.42-355029.7 and CWISE J233531.55+014219 (see below). Parallaxes were updated in the data compilation for all high-probability T dwarf companions identified by Rothermich et al. (2024), using the more precise values for the primaries. The updated parallaxes presented by Beiler et al. (2024) for CWISEP J104756.81+545741.6 and CWISEP J144606.62-231717.8 were also included. The complete dataset is given in the Appendix.

We reviewed the W3 magnitudes in our compilation and redetermined several values. We redetermined W3 for all values with an uncertainty  $\geq 0.25$  magnitudes (51 sources), and we also redetermined W3 for sources brighter than 12 with an error larger than 0.15 magnitudes (an additional 11 sources). We redetermined W3 for the faint Y dwarf WISE J035934.06-540154.6 where the estimated uncertainty seemed too small given the faintness of the source. Finally, we examined the images for sources bright enough for an AllWISE W3 detection but with no W3 measurement reported, and determined values for three sources.

W3 images were downloaded as FITS files from the IRSA *WISE* image service and aperture photometry was carried out; the data were calibrated using the zeropoint given in the headers. Care was taken to exclude any nearby sources, using small apertures as necessary and determining the aperture correction using bright isolated stars in the same image. Care was also taken to make sure the sky estimate was appropriate for the location of the brown dwarf. The sky estimate is the largest source of uncertainty as the *WISE* W3 image pixels are large, the background is high, and the background is spatially variable. The uncertainty in W3 was estimated from the scatter in the background measurements.

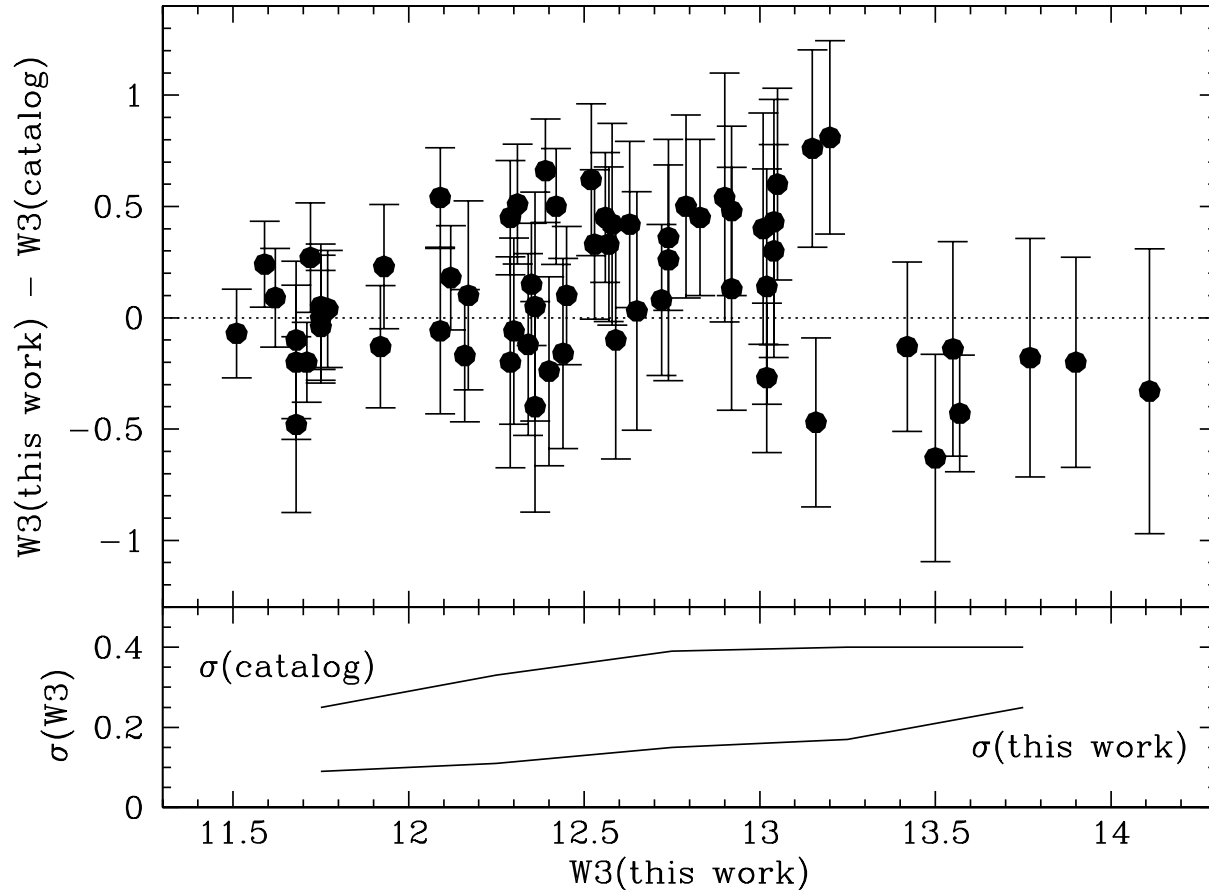


**Figure 3.** The top panel shows the difference between the previously available W3 magnitudes and those measured in this work, for 63 brown dwarfs. The lower panel shows the uncertainties in the W3 magnitudes averaged over 0.5 magnitude bins.

Table 1 gives revised W3 values for 66 brown dwarfs, and Table 2 lists 16 brown dwarfs whose previously quoted W3 magnitudes were found to be invalid on image inspection, due to source blending or the field being too crowded for confident identification of the source. Figure 3 shows the differences between the 63 old and new W3 magnitudes, and the estimated uncertainties as a function of W3. There is no clear trend in the differences, and the measurements presented here are significantly more precise.

**Table 1.** Revised W3 Magnitudes

| AllWISE Name       | Previous mag |      | Revised mag |      |
|--------------------|--------------|------|-------------|------|
|                    | W3           | err  | W3          | err  |
| 000517.48+373720.5 | 11.79        | 0.24 | 11.75       | 0.08 |

**Table 1** continued on next page

**Table 1** (*continued*)

| AllWISE Name<br>Jhhmmss.ss±ddmmss.s | Previous mag |      | Revised mag |      |
|-------------------------------------|--------------|------|-------------|------|
|                                     | W3           | err  | W3          | err  |
| 001449.96+795116.1                  | 13.69        | 0.40 | 13.55       | 0.27 |
| 002810.59+521853.1                  | 13.95        | 0.43 | 13.77       | 0.32 |
| 003452.03+052306.9                  | 11.78        | 0.31 | 11.68       | 0.17 |
| 003829.06+275852.0                  | 12.38        | 0.33 | 12.83       | 0.12 |
| 004143.14-401924.3                  | 12.36        | 0.39 | 12.30       | 0.15 |
| 004945.61+215120.0                  | 11.58        | 0.19 | 11.51       | 0.06 |
| 005021.05-332228.8                  | 11.84        | 0.24 | 12.29       | 0.09 |
| 010650.61+225159.1                  | 12.49        | 0.46 | 12.29       | 0.11 |
| 013217.78-581825.9                  | 14.10        | 0.40 | 13.90       | 0.25 |
| 014603.23-261908.7                  | 13.63        | 0.34 | 13.16       | 0.17 |
| 014837.52-104803.9                  | 12.69        | 0.52 | 12.59       | 0.12 |
| 030919.70-501614.2AB                | 12.76        | 0.46 | 12.36       | 0.11 |
| 031326.00+780744.3                  | 12.05        | 0.26 | 11.92       | 0.09 |
| 032547.73+083118.2                  | 11.88        | 0.34 | 11.68       | 0.07 |
| 035000.31-565830.5                  | 12.33        | 0.28 | 12.16       | 0.10 |
| 035934.06-540154.6                  | 14.00        | 0.20 | 13.57       | 0.17 |
| 041022.75+150247.9                  | 12.31        | 0.50 | 12.36       | 0.12 |
| 041102.17+471423.6                  | 12.36        | 0.50 | 12.90       | 0.25 |
| 062720.07-111428.0                  | 11.53        | 0.21 | 11.62       | 0.07 |
| 075108.79-763449.6                  | 11.91        | 0.16 | 11.71       | 0.08 |
| 081117.95-805141.4                  | 12.64        | 0.32 | 12.72       | 0.11 |
| 094306.00+360723.3                  | 12.29        | 0.39 | 12.79       | 0.13 |
| 095047.31+011733.1                  |              |      | 12.50       | 0.12 |
| 104053.42-355029.7                  | 12.62        | 0.52 | 12.65       | 0.13 |
| 105349.41-460241.2                  | 14.13        | 0.40 | 13.50       | 0.24 |
| 105512.93+544329.7                  | 11.55        | 0.20 | 12.09       | 0.10 |
| 111448.74-261827.9                  | 11.35        | 0.18 | 11.59       | 0.07 |
| 111838.69+312537.7                  | 12.24        | 0.33 | 12.57       | 0.11 |
| 114156.67-332635.5                  | 11.73        | 0.21 | 12.39       | 0.10 |
| 115013.85+630241.3                  | 12.38        | 0.30 | 12.74       | 0.13 |

**Table 1** *continued on next page*

**Table 1** (*continued*)

| AllWISE Name<br>Jhhmmss.ss±ddmmss.s | Previous mag |      | Revised mag |      |
|-------------------------------------|--------------|------|-------------|------|
|                                     | W3           | err  | W3          | err  |
| 115229.63+035926.8                  | 12.48        | 0.50 | 12.74       | 0.21 |
| 121710.27-031112.1                  | 11.70        | 0.26 | 11.93       | 0.10 |
| 123738.95+652620.3                  | 11.94        | 0.22 | 12.12       | 0.08 |
| 125721.01+715349.3                  | 13.55        | 0.33 | 13.42       | 0.19 |
| 125804.91-441232.6                  | 12.11        | 0.27 | 12.56       | 0.11 |
| 130041.63+122114.5                  | 11.70        | 0.27 | 11.75       | 0.08 |
| 130217.08+130851.0                  | 12.16        | 0.42 | 12.58       | 0.17 |
| 133553.41+113004.7                  | 12.15        | 0.36 | 12.09       | 0.09 |
| 134646.07-003151.4                  | 11.92        | 0.24 | 12.42       | 0.10 |
| 140518.32+553421.3                  | 12.20        | 0.26 | 12.35       | 0.09 |
| 144901.84+114710.7                  | 12.74        | 0.45 | 13.04       | 0.16 |
| 145731.67+472420.1                  | 12.64        | 0.41 | 12.40       | 0.11 |
| 150411.80+102715.6                  | 12.60        | 0.41 | 12.44       | 0.12 |
| 150457.56+053759.8                  |              |      | 12.65       | 0.12 |
| 154151.70-225019.1                  | 12.20        | 0.30 | 12.53       | 0.15 |
| 162414.07+002915.6                  | 12.16        | 0.39 | 11.68       | 0.06 |
| 162838.09+230822.7                  | 11.80        | 0.25 | 12.31       | 0.10 |
| 170745.84-174452.4                  | 12.07        | 0.41 | 12.17       | 0.11 |
| 173835.52+273258.8                  | 12.45        | 0.40 | 13.05       | 0.16 |
| 175805.45+463316.9                  | 12.35        | 0.29 | 12.45       | 0.11 |
| 181006.18-101000. 5                 | 11.45        | 0.22 | 11.72       | 0.11 |
| 182831.08+265037.6                  | 12.44        | 0.34 | 12.92       | 0.17 |
| 183207.94-540943.3                  | 12.61        | 0.52 | 13.04       | 0.18 |
| 193054.55-205949.4                  | 14.44        | 0.58 | 14.11       | 0.27 |
| 200520.35+542433.6                  | 12.39        | 0.40 | 13.20       | 0.17 |
| 205628.91+145953.2                  | 11.73        | 0.25 | 11.77       | 0.08 |
| 213456.79-713744.7                  | 12.39        | 0.40 | 13.15       | 0.19 |
| 220905.75+271143.6                  | 12.46        | 0.39 | 12.34       | 0.12 |
| 222829.01-431029.8                  | 11.75        | 0.27 | 11.75       | 0.08 |
| 223204.53-573010.4                  | 11.90        | 0.32 | 12.52       | 0.12 |

**Table 1** *continued on next page*

**Table 1** (*continued*)

| AllWISE Name<br>Jhhmmss.ss±ddmmss.s | Previous mag |      | Revised mag |      |
|-------------------------------------|--------------|------|-------------|------|
|                                     | W3           | err  | W3          | err  |
| 225404.16-265257.5                  | 13.29        | 0.29 | 13.02       | 0.17 |
| 230158.29-645857.5                  | 12.61        | 0.48 | 13.01       | 0.20 |
| 233531.55+014219.6                  |              |      | 12.81       | 0.20 |
| 234351.20-741846.9                  | 12.79        | 0.50 | 12.92       | 0.22 |
| 235120.61-700025.7                  | 12.88        | 0.51 | 13.02       | 0.14 |

**Table 2.** Excluded W3 magnitudes Due to Source Confusion or Blending

| AllWISE Name       | AllWISE Name       | AllWISE Name       |
|--------------------|--------------------|--------------------|
| 003231.09-494651.4 | 080622.22-082046.4 | 145838.12+173447.7 |
| 003507.79-153230.7 | 083019.97-632305.4 | 181849.69-470146.4 |
| 004158.29+381811.9 | 094005.50+523359.2 | 214025.23-332707.4 |
| 032517.68-385453.8 | 132233.63-234017.0 | 235716.49+122741.5 |
| 071322.55-291752.0 | 141127.88-481151.5 |                    |
| 072719.15+170951.3 | 141623.96+134836.0 |                    |

### 3. ANALYSIS

#### 3.1. Models

Over the last 20 years significant improvements have been made in modelling the atmospheres of cool stars and brown dwarfs. These include more complete molecular line lists (e.g. [Saumon et al. 2012](#); [Yurchenko & Tennyson 2014](#); [Polyansky et al. 2018](#)), a better understanding of vertical mixing and the resulting disequilibrium chemistry (e.g. [Saumon et al. 2006](#); [Zahnle & Marley 2014](#)), and the incorporation of grain formation and sedimentation (e.g. [Ackerman & Marley 2001](#); [Morley et al. 2012, 2014](#); [Lacy & Burrows 2023](#)). However, while synthetic spectra and photometry reproduced the observations of cool stars and brown dwarfs with  $T_{\text{eff}} > 600$  K, systematic discrepancies of  $\approx 50\%$  existed at wavelengths around  $1.2 \mu\text{m}$  and at 2 to  $4 \mu\text{m}$ , for cooler brown dwarfs (e.g. [Leggett et al. 2017](#); [Karalidi et al. 2021](#); [Lacy & Burrows 2023](#)); the modelled near-infrared flux was typically too bright and the 2 to  $4 \mu\text{m}$  flux was typically too faint.



For cold brown dwarfs, the near-infrared flux emerges from layers deep in the atmosphere, and the 2 to 4  $\mu\text{m}$  flux emerges from higher layers (e.g. Karalidi et al. 2021, their Figure 17). Knowing this, Leggett et al. (2021) explored modifications to the standard radiative/convective, adiabatic, pressure-temperature relationship, in order to make the lower atmosphere colder and the upper atmosphere warmer. The atmospheric structure was parameterized by a pressure  $P_{(\gamma, \text{max})}$ , defining the atmospheric depth above which the adiabatic parameter  $\gamma$  is less than the standard value ( $\approx 1.4$  for hydrogen). Tuning the models to reproduce the  $1 \lesssim \lambda \mu\text{m} \lesssim 20$  energy distributions of one T9 dwarf and six Y dwarfs, values of  $\gamma$  between 1.20 and 1.33 were derived, with  $7 \lesssim P_{(\gamma, \text{max})} \text{ bar} \lesssim 50$ . Using the modified adiabat improved agreement with spectroscopic and photometric observations of cold brown dwarfs by factors of two to five at  $1 \lesssim \lambda \mu\text{m} \lesssim 5$  (Leggett et al. 2021, Figures 12 and 13).

The  $P_{(\gamma, \text{max})}$  layer for the Leggett et al. (2021) sample corresponded to temperatures around 800 K, a region where the gaseous nitrogen chemistry is changing and chlorides and sulfides are condensing (Lodders 1999; Morley et al. 2012; Leggett et al. 2021), possibly disrupting convection and leading to a diabatic profile. The rapid rotation of the cool brown dwarfs (Zapatero Osorio et al. 2006; Tannock et al. 2021) is also expected to alter the pressure-temperature profile of the atmosphere (e.g. Tan & Showman 2021, their Figure 4). Retrieval analyses have determined similar changes to the atmospheric profile, see Kothari et al. (2024); Lew et al. (2024) for recent examples using *JWST* data.

Leggett et al. (2021) generate a grid of models which include disequilibrium chemistry and adopt a diabatic profile with an effective adiabatic parameter of  $\gamma = 1.25$  and  $P_{(\gamma, \text{max})} = 15$  bar; these are known as the ATMO 2020++ model atmospheres. Note that the adopted values for  $\gamma$  and  $P_{(\gamma, \text{max})}$  are empirical and based on the fit to the energy distributions, they have not been quantitatively connected to a diabatic or kinetic process.

The ATMO 2020++ grid was expanded to include a wider range in metallicity for Meisner et al. (2023). Later, a grid of phosphine-free ATMO 2020++ models was generated for Leggett & Tremblin (2023, 2024) because *JWST* data show it to be absent (Beiler et al. 2023; Leggett & Tremblin 2023; Lew et al. 2024; Luhman et al. 2024). Phosphine is a chemical disequilibrium species which is expected to be the stable form of phosphorus in cool atmospheres (Visscher et al. 2006); although the feature is seen in solar system giant planets, it may be that the different composition or gravity of the brown dwarf atmosphere results in phosphorus taking a different form. ATMO 2020++ synthetic spectra and colors are available on the ERC ATMO OpenData web site<sup>1</sup>.

We use the phosphine-free ATMO 2020++ models in this work. The adiabat is modified at atmospheric pressures between 0.15 and 15 bars at  $\log g = 4.5$ , which are scaled by  $\times 10^{(\log g - 4.5)}$  at other surface gravities. Out-of-equilibrium chemistry is used with  $K_{zz} = 10^5 \text{ cm}^2 \text{ s}^{-1}$  at  $\log g = 5.0$ , which is scaled by  $\times 10^{2(5 - \log g)}$  at other surface gravities. The model grid covers  $250 \leq T_{\text{eff}} \text{ K} \leq 1200$  (250 K, 275 K, 300 K, 350 K, 400 K, 450 K, 500K, then every 100 K to 1200 K), for three metallicities:  $[\text{m}/\text{H}] = -0.5, 0, +0.3$ .

Our brown dwarf sample is local – 90% of the brown dwarfs with measured distances lie within 25 pc – and a range in metallicity between  $-0.5$  and  $+0.3$  covers the likely range of values for the population (e.g. Hinkel et al. 2014, their Figure 4). Evolutionary models calculate that brown dwarfs with  $T_{\text{eff}}$  values between 300 K and 800 K, and a likely age range of 0.5 Gyr to 6 Gyr (Dupuy &

<sup>1</sup> <https://opendata.erc-atmo.eu>

Liu 2017; Kirkpatrick et al. 2021a; Best et al. 2024), have a range in  $\log g$  of 3.5 to 5.0 (Marley et al. 2021). The metal-poor grid includes  $\log g$  values of 4.0, 4.5 and 5.0; the solar metallicity grid includes  $\log g$  values of 3.5, 4.0, 4.5 and 5.0; and the metal-rich grid includes  $\log g$  values of 2.5 to 5.5 in steps of 0.5 dex.

### 3.2. Sensitivity to Metallicity and Gravity

Figure 2 shows a synthetic 450 K spectrum for a brown dwarf at 10 pc, with radii determined from evolutionary models for each  $T_{\text{eff}}$  and gravity (Marley et al. 2021). *JWST* and *WISE* filter profiles are overlaid. The spectrum is also shown divided by spectra with the same  $T_{\text{eff}}$  but with lower gravity (middle panel) and lower metallicity (bottom panel). The radius of the  $\log g = 4.0$  brown dwarf is  $1.35\times$  larger than the  $\log g = 5.0$  brown dwarf, meaning an increase in brightness of 80%. Without the radius adjustment the red comparison line in the middle panel of Figure 2 would lie at  $y \approx 0.6$ .

Figure 2 shows that the near-infrared region is very sensitive to both metallicity and gravity, as previously noted for T dwarfs (e.g. Burgasser et al. 2006a; Liu et al. 2007) and Y dwarfs (e.g. Leggett et al. 2017). The  $10 \lesssim \lambda \mu\text{m} \lesssim 15$  region shows some sensitivity to metallicity and gravity but not to the same degree. Interestingly, the average flux over the W2 (or F444W) bandpass is approximately equal in all three cases. The absorption features at these wavelengths (primarily due to CO and CO<sub>2</sub>) increase with decreasing gravity, however the increase in radius compensates for the additional absorption, at this temperature.

Figure 4 illustrates the gravity and metallicity sensitivity for cold brown dwarfs using the W2 – W3 color, with  $M_{W2}$  or  $J - W2$  as a proxy for  $T_{\text{eff}}$ . As  $T_{\text{eff}}$  decreases below 600 K the intrinsic spread of the W2 – W3 color increases significantly, primarily caused by an increase in sensitivity to gravity. For Y dwarfs, with  $T_{\text{eff}} \lesssim 500$  K, the W2 – W3 color increases by 0.3 to 0.6 magnitudes for a 0.5 dex decrease in  $\log g$ . A 0.5 dex decrease in  $[\text{m}/\text{H}]$  results in smaller changes of 0.1 to 0.3 magnitudes. Brown dwarfs (or exoplanets) with very blue or very red W2 – W3 colors are identified in the figure and discussed in detail below.

Note also that for Y dwarfs warmer than  $\sim 400$  K,  $M_{W2}$  changes very little ( $\sim 20\%$ ) as gravity and metallicity are varied and  $T_{\text{eff}}$  kept constant. Hence  $M_{W2}$  (or a similar bandpass) can be a useful luminosity indicator.

### 3.3. Candidate Young, Very Low Mass Brown Dwarfs or Exoplanets

Ten sources are identified in Figure 4 which lie along or redwards of the  $\log g = 3.5$  sequences. Their  $M_{W2}$  and  $J - W2$  colors indicate  $500 \lesssim T_{\text{eff}} \text{ K} \lesssim 800$ . Evolutionary models then imply young ages of 10 to 80 Myr and a low mass of around  $3 M_{\text{Jup}}$  (see e.g. Figure 10 of Marley et al. 2021). These young objects may also be metal-rich, however a metallicity  $\gg +0.3$  dex is unlikely for this local sample (e.g. Nordström et al. 2004; Rojas-Ayala et al. 2012; Hinkel et al. 2014). Each source is discussed below, and a summary of their properties is given in Table 3.

Three of the objects have kinematics consistent with membership of the Carina-Near moving group with an age of  $\sim 200$  Myr (Gagné et al. 2018): WISE J001449.85+795115.9, T8; ULAS J130217.21+130851.2, T8.5; CWISE J233531.55+014219.6, T9. A parallax measurement would strengthen the case for group membership for WISE J001449.85+795115.9, where the 77% likelihood is based on location and proper motion only. Zhang et al. (2021) report that ULAS

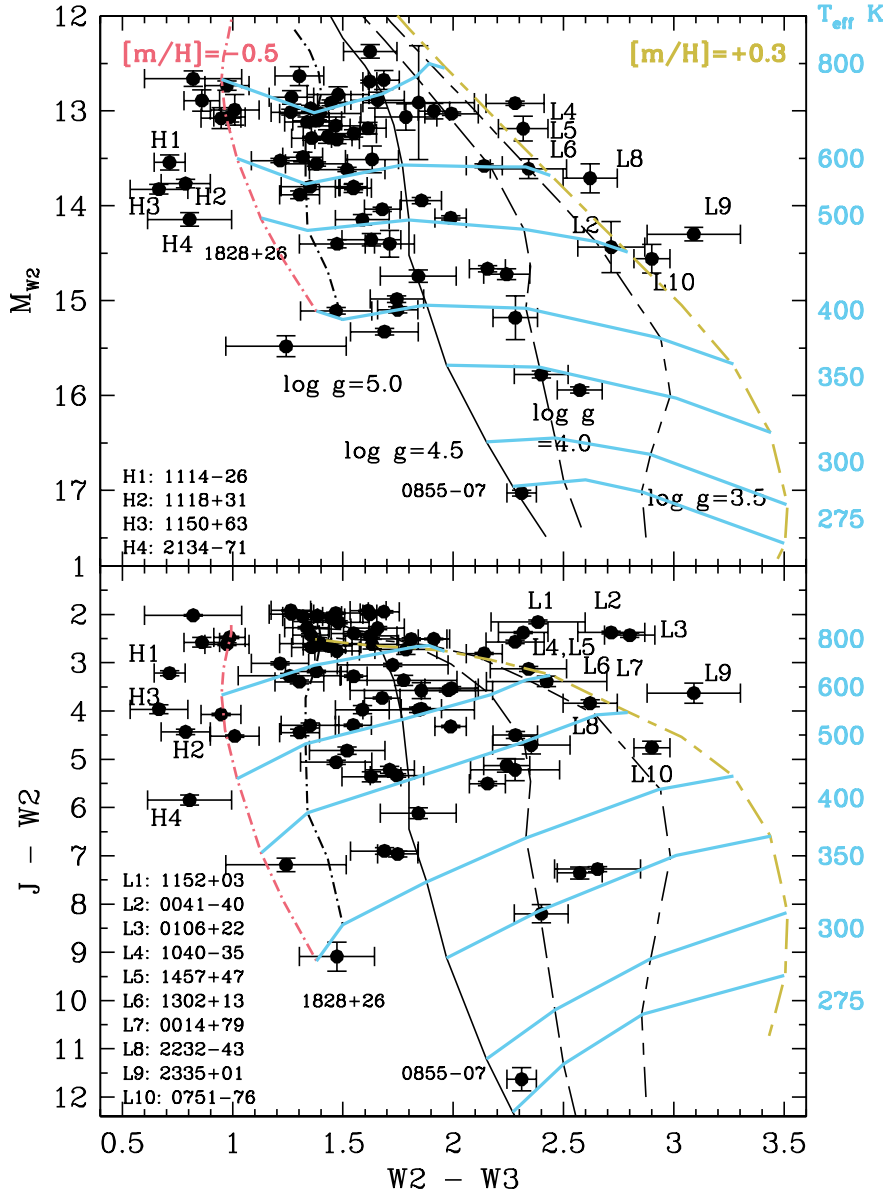


**Figure 4.** Color magnitude diagrams for late-T and Y dwarfs. Black circles are data points from the compilation presented here. Sources with extreme  $W2 - W3$  colors are identified by an abbreviated *WISE* RA-Decl. The locations of the unusual Y dwarf WISEPA J182831.08+265037.8, and the very cold WISE J085510.83-071442.5, are also indicated. Black almost vertical lines are solar metallicity ATMO 2020++ PH<sub>3</sub>-free sequences for  $\log g = 3.5, 4.0, 4.5,$  and  $5.0$  from right to left. The red line is a  $\log g = 5.0$  sequence with  $[m/H] = -0.5$  and the yellow line is a  $\log g = 3.5$  sequence with  $[m/H] = +0.3$ . The cyan lines are isotherms, with  $T_{\text{eff}}$  indicated along the right axes. At these temperatures,  $\log g = 3.5$  corresponds to a mass of  $\approx 3M_{Jup}$ ,  $4.0$  to  $\approx 6M_{Jup}$ ,  $4.5$  to  $\approx 14M_{Jup}$ , and  $5.0$  to  $\approx 35M_{Jup}$  (Marley et al. 2021). Temperature decreases with age for a given mass; an age of 15 Gyr corresponds to  $T_{\text{eff}}$  values of 400 K and 260 K for  $\log g = 5.0$  and  $4.5$  respectively, and colder values for lower gravities (Marley et al. 2021).

J130217.21+130851.2 has much redder  $J - K$  and  $H - K$  colors than other T8 – T9 field dwarfs, and has slightly enhanced fluxes near the  $Y$ -band peak, suggesting a lower surface gravity. [Rothermich et al. \(2024\)](#) report that CWISE J233531.55+014219.6 is a companion to the triple K and M dwarf system GJ 900, and that the age of the system (based on rotational measurements) is 100 – 300 Myr.

The T9 WISEP J075108.79-763449.6, also known as COCONUTS-2b or L 34-26b ([Zhang et al. 2021](#)), is the coolest source. Although its kinematics do not associate it with any young moving group, the tangential velocity is low at 11 km s<sup>-1</sup>, supporting classification as a young field dwarf ([Zhang et al. 2021](#)). [Zhang et al. \(2021\)](#) estimate an age for the solar-metallicity M dwarf primary using its spectroscopic, activity, rotation, kinematic, and photometric properties; they determine an age of 150 — 800 Myr for the system. Those authors estimate the luminosity of the secondary from its near-infrared magnitudes, and combine this with the age estimate to constrain the temperature, gravity and mass of the secondary to  $T_{\text{eff}} = 434 \pm 9\text{K}$ ,  $\log g = 4.11^{+0.11}_{-0.18}$ ,  $\text{mass} = 6.3^{+1.5}_{-1.9} M_{\text{Jup}}$ , from

**Table 3.** Estimated Properties of Candidate Young 3  $M_{\text{Jup}}$  Objects

| AllWISE Name                      | Other Name(s)            | $T_{\text{eff}}$ K | Age Myr  |
|-----------------------------------|--------------------------|--------------------|----------|
| 001449.85+795115.9 <sup>a</sup>   |                          | 600                | 10 – 100 |
| 004143.77-401929.9                |                          | 500 – 800          | 10 – 40  |
| 010650.61+225159.1                |                          | 800                | 4 – 10   |
| 075108.79-763449.6 <sup>b</sup>   | COCONUTS-2b, L 34-26b    | 450                | 30 – 80  |
| 104053.42-355029.7                | UPM J1040-3551b          | 700                | 10 – 30  |
| 115229.64+035926.8                | ULAS J115229.67+035927.2 | 800                | 5 – 15   |
| 130217.21+130851.2 <sup>a</sup>   |                          | 600                | 20 – 40  |
| 145731.67+472420.1 <sup>c</sup>   | PSO J224.3820+47.40      | 700                | 10 – 30  |
| 223204.50-573010.5                |                          | 550                | 15 – 40  |
| 233531.55+014219.6 <sup>a,d</sup> | GJ 900b                  | 500                | 15 – 40  |

NOTE—

$T_{\text{eff}}$  is estimated from the isotherms shown in Figure 4; age is estimated from evolutionary models ([Marley et al. 2021](#)), adopting this  $T_{\text{eff}}$  and  $\log g \approx 3.5$ , and taking into account the error bars shown in Figure 4. Estimated uncertainties are  $\sim 50$  K and  $\sim 50\%$  in age (however see other age estimates in the following notes).

<sup>a</sup> Kinematics suggest membership of the Carina-Near moving group with an age of  $\sim 200$  Myr ([Gagné et al. 2018](#)).

<sup>b</sup> [Zhang et al. \(2021\)](#) estimate an age of 150 — 800 Myr using the M dwarf primary; for the brown dwarf they use a luminosity estimate to determine:  $T_{\text{eff}} = 434\text{K}$ ,  $\log g = 4.11$ ,  $\text{mass} = 6.3 M_{\text{Jup}}$ .

<sup>c</sup> Near-infrared spectral analyses by [Zhang et al. \(2021\)](#) and [Zalesky et al. \(2022\)](#) find  $T_{\text{eff}} \approx 900$  K,  $\log g \approx 3.7$ , implying a mass and age of  $\sim 4 M_{\text{Jup}}$  and  $\sim 15$  Myr from evolutionary models ([Marley et al. 2021](#)).

<sup>d</sup> A companion to the triple system GJ 900, with an age based on rotational measurements of 100 – 300 Myr ([Rothermich et al. 2024](#)).

both hot- and cold-start evolutionary models. These properties are consistent with the location of the source in Figure 4. WISEP J075108.79-763449.6 has been observed by *JWST* as part of program 3514, PI Mickael Bonnefoy, and therefore the properties of this interesting source should soon be better known.

WISE J145731.67+472420.1 (also PSO J224.3820+47.4057) is classified as a T7 dwarf by Best et al. (2015). Near-infrared spectral analyses appear to confirm the low gravity indicated in Figure 4. Forward modelling by Zhang et al. (2021) assigns  $T_{\text{eff}} = 921 \pm 4\text{K}$  and  $\log g = 3.67^{+0.32}_{-0.01}$ , while a retrieval analysis by Zalesky et al. (2022) finds  $T_{\text{eff}} = 893^{+9}_{-26}\text{K}$ ,  $\log g = 3.65^{+0.25}_{-0.14}$ . Evolutionary models (Marley et al. 2021) then provide mass and age estimates of  $\sim 4 M_{\text{Jup}}$  and  $\sim 15$  Myr. The parallax and proper motion (Best et al. 2020) give a low tangential velocity of  $16 \text{ km s}^{-1}$ , supporting a young age (e.g. Dupuy & Liu 2012, their Figure 31), although the BANYAN tool (Gagné et al. 2018) assigns field membership.

The remaining five young planetary-mass candidates require additional observations to confirm their nature:

- CWISE J004143.77-401929.9 is classified as a T8-peculiar by Kirkpatrick et al. (2021a), and it has an enhanced *K*-band flux, suggestive either of low gravity or high metallicity, or both. The BANYAN tool (Gagné et al. 2018) estimates field membership for this source, that is, not young, and the tangential velocity is high at  $95 \text{ km s}^{-1}$ , which would also not support a young age (e.g. Dupuy & Liu 2012, their Figure 31). However the location of the source in the two panels of Figure 4 is inconsistent. Agreement would be improved if the trigonometric parallax is underestimated and the target is closer than inferred from the parallax; this would also reduce the tangential velocity. An improved parallax measurement and *JWST* observations would help constrain the nature of this source.
- CWISEP J010650.61+225159.1 is classified as a T6.5 dwarf by Meisner et al. (2020a). There is no published trigonometric parallax or near-infrared spectrum. Both of these would be useful. The BANYAN tool (Gagné et al. 2018) estimates field membership for this source based on location and proper motion alone.
- CWISE J104053.42-355029.7 is classified as a T7 dwarf by Rothermich et al. (2024), who also determine that it is a wide companion to the M dwarf UPM J1040-3551 (or 2MASS J1040549-3551311), which has a metallicity close to solar ( $[\text{Fe}/\text{H}] \approx -0.06$ ). The tangential velocity is low at  $15 \text{ km s}^{-1}$ , possibly supporting a young age (e.g. Dupuy & Liu 2012, their Figure 31), although the BANYAN tool (Gagné et al. 2018) assigns a field membership. Further studies of the M dwarf primary, to constrain the age of the system, would be valuable.
- ULAS J115229.67+035927.2 is classified as a T6 by Scholz et al. (2012); the near-infrared spectrum appears typical for its type. The proper motion of the source is very uncertain, and there is no published trigonometric parallax measurement; the BANYAN tool (Gagné et al. 2018) is unable to constrain moving group membership. Additional astrometry and a parallax measurement would be helpful for this source.
- WISE J223204.50-573010.5 is classified as a T9 dwarf by Tinney et al. (2018), and the tangential velocity (Kirkpatrick et al. 2019) of  $39 \text{ km s}^{-1}$ , suggests thin disk membership (e.g. Dupuy &



Liu 2012, their Figure 31); the BANYAN tool (Gagné et al. 2018) assigns field membership. A near-infrared spectrum covering the  $K$ -band would be helpful, as would  $JWST$  data.

### 3.4. Candidate Old and Metal-Poor Brown Dwarfs

Four sources are identified in Figure 4 with  $W2 - W3 \approx 0.7$  and  $14.2 \geq M_{W2} \geq 13.5$ , implying  $500 \leq T_{\text{eff}} \text{ K} \leq 600$ . The models indicate that they have  $\log g > 5$  and are significantly metal-poor. Evolutionary models then imply an age  $\geq 8$  Gyr and a mass  $\geq 35 M_{\text{Jup}}$ .

One of these sources, WISE J111838.70+312537.9, is a T8.5 member of the  $\xi$  Ursae Majoris system (Wright et al. 2013). Wright et al. (2013), and references therein, report  $[\text{Fe}/\text{H}] = -0.32$  for the system and an age between 2 and 8 Gyr. These are consistent with the model inferences above, if the age is towards the higher limit.

The other three sources are known metal-poor brown dwarfs, from studies by Zhang et al. (2019); Zhang et al. (2021) using near-infrared spectroscopy and model analyses: WISEA J111448.74-261827.9, T7.5; WISE J115013.85+630241.5, T8; and WISEP J213456.73-713743.6, T9pec. Zhang et al. (2021) estimate  $[\text{m}/\text{H}] \approx -0.4$  for WISEA J111448.74-261827.9, a value which appears typical for the T dwarfs in their samples. These sources all have a tangential velocity of  $\lesssim 60 \text{ km s}^{-1}$  suggesting thin disk membership (e.g. Dupuy & Liu 2012, their Figure 31) and an age not significantly higher than 8 Gyr (e.g. Haywood et al. 2013).

### 3.5. The Unusual Y Dwarf WISEPA J182831.08+265037.8

The Y dwarf WISEPA J182831.08+265037.8 (hereafter WISE 1828) has been recognized to be unusual since its discovery by Cushing et al. (2011). Historically, it was a challenge to reproduce the observations using the then available models (e.g. Beichman et al. 2013). Also, although its superluminosity suggests multiplicity,  $JWST$  images exclude a companion at distances  $> 0.5$  au (De Furio et al. 2023). In our previous analysis using ATMO 2020++ models, we estimated that the system is likely to be an identical pair of brown dwarfs with  $T_{\text{eff}} = 375 \text{ K}$ ,  $\log g = 4.0$ , and  $[\text{m}/\text{H}] = -0.5$  (Leggett et al. 2021). That fit was based on a near-infrared spectrum and mid-infrared photometry.

In this work we revise the W3 photometry for WISE 1828 (Section 2, Table 1). The bluer  $W2 - W3$  color places this dwarf on the  $\log g = 5$  model sequence in Figure 4. While the  $M_{W2}:W2-W3$  plot (upper panel of Figure 4) suggests it could be a single 500 K brown dwarf, the  $J - W2:W2-W3$  plot (lower panel) implies  $T_{\text{eff}} \approx 400 \text{ K}$ ; the colors are consistent if the source is a 400 K binary composed of near-identical dwarfs. Moderate resolution mid-infrared spectra are now available for WISE 1828, and we can use these data to further explore the use of the  $W2 - W3$  color as a gravity indicator. Lew et al. (2024) present 2.9 to 5.1  $\mu\text{m}$  NIRSpect spectra, and Barrado et al. (2023) present 4.9 to 18  $\mu\text{m}$  MIRI spectra. Figure 5 compares the observed NIRSpect and MIRI spectra to various ATMO 2020++ PH<sub>3</sub>-free synthetic spectra. We use the measured distance to the dwarf, and constrain the radius to be equal to the evolutionary model values (Marley et al. 2021), to scale the synthetic spectra to the observations.

We explored binary solutions to the observed NIRSpect and MIRI spectra, given that the  $J, W2, W3$  color-set can only be reproduced if the system is a pair of near-identical 400 K dwarfs (Figure 4). The colors are matched by ATMO 2020++ model atmospheres with  $\log g = 4.5$  or 5.0, solar or sub-solar metallicity, and  $350 < T_{\text{eff}} \text{ K} < 450$  (Figure 4); we restricted comparison spectra to those parameter ranges, as available in our grid (Section 3.1).

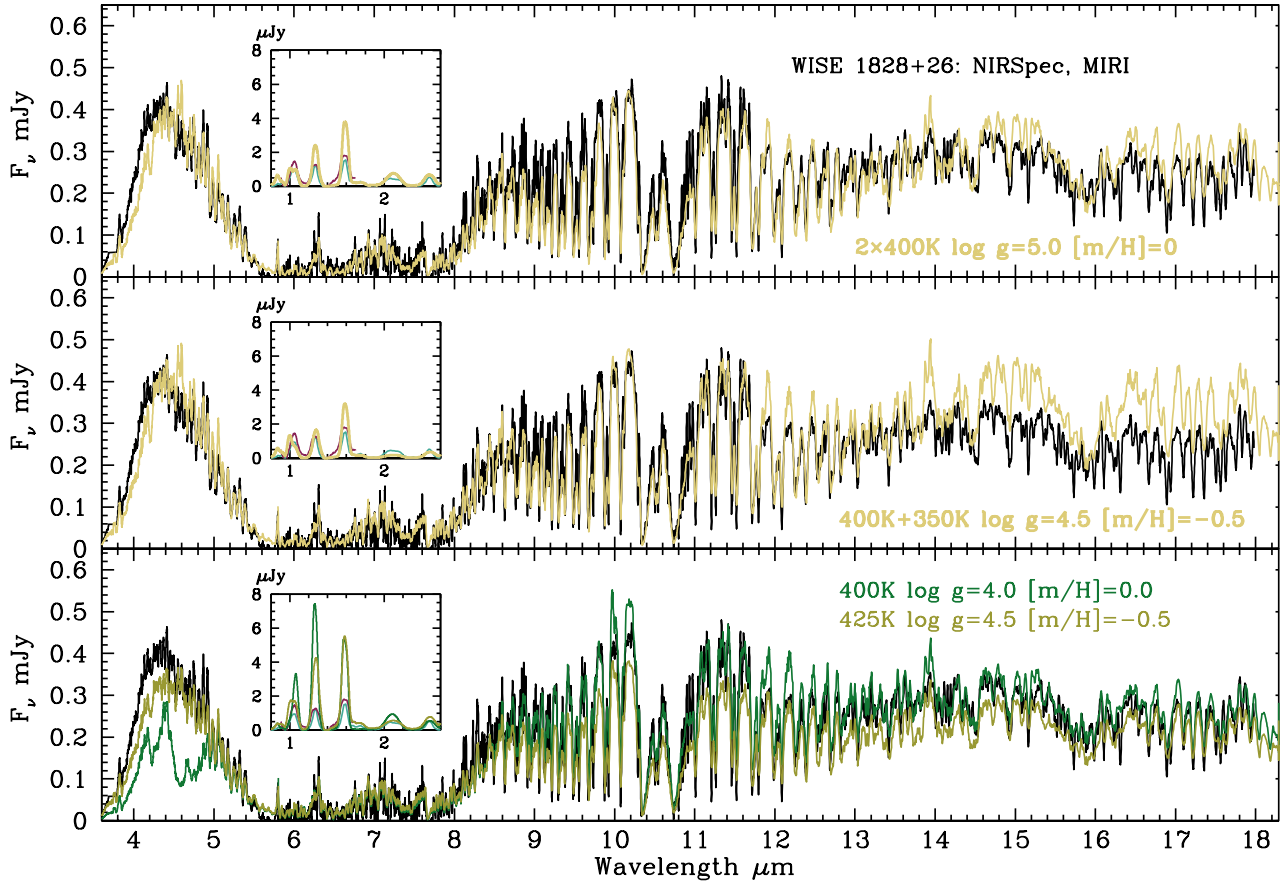


**Figure 5.** The black lines are *JWST* NIRSpec and MIRI data for WISEPA J182831.08+265037.8, from Barrado et al. (2023) and Lew et al. (2024). The insets show the near-infrared region, where cyan lines are the low-resolution NIRSpec data (*JWST* Cycle 1 GTO program 1189, PI Thomas Roellig) and red lines are *Hubble Space Telescope* data from Cushing et al. (2021). Yellow, olive and green lines are ATMO 2020++ PH<sub>3</sub>-free synthetic spectra, with parameters given in the legends; yellow spectra adopt a binary solution, the olive and green spectra are for a single dwarf. Scaling the synthetic spectra is done by adopting the brown dwarf radius as calculated by evolutionary models (Marley et al. 2021) for each  $T_{\text{eff}}$  and  $\log g$ , and using the measured distance to the Y dwarf. The upper two panels reproduce the observations quite well, with the top spectrum being our preferred solution. In the bottom panel, the olive line is an ATMO 2020++ synthetic spectrum with parameters similar to the Lew et al. (2024) Elf-Owl fit to the  $2.9 \lesssim \lambda \mu\text{m} \lesssim 5.1$  NIRSpec spectrum. The green line is the ATMO 2020++ synthetic spectrum adopted by Barrado et al. (2023) as the best-fit ATMO model to their  $5.0 \lesssim \lambda \mu\text{m} \lesssim 18$  MIRI spectrum. See text for further discussion.

We interpolated the observations and the synthetic spectra to a sampling frequency of  $\delta\lambda = 0.0025 \mu\text{m}$  and calculated Goodness-of-Fit (GF) statistics for each solution by summing the squares of the difference between the observed and modelled flux, divided by the uncertainty in the observed flux. We explored using different wavelength regions for the GF calculation, avoiding wavelengths where there is very little signal. The best fits were found for the two binary solutions shown in the top panels of Figure 5: (1) a pair of 400 K,  $\log g = 5.0$ ,  $[\text{m}/\text{H}] = 0$  brown dwarfs, and (2) a system composed of a 400 K and a 350 K brown dwarf, both with  $\log g = 4.5$  and  $[\text{m}/\text{H}] = -0.5$ . The

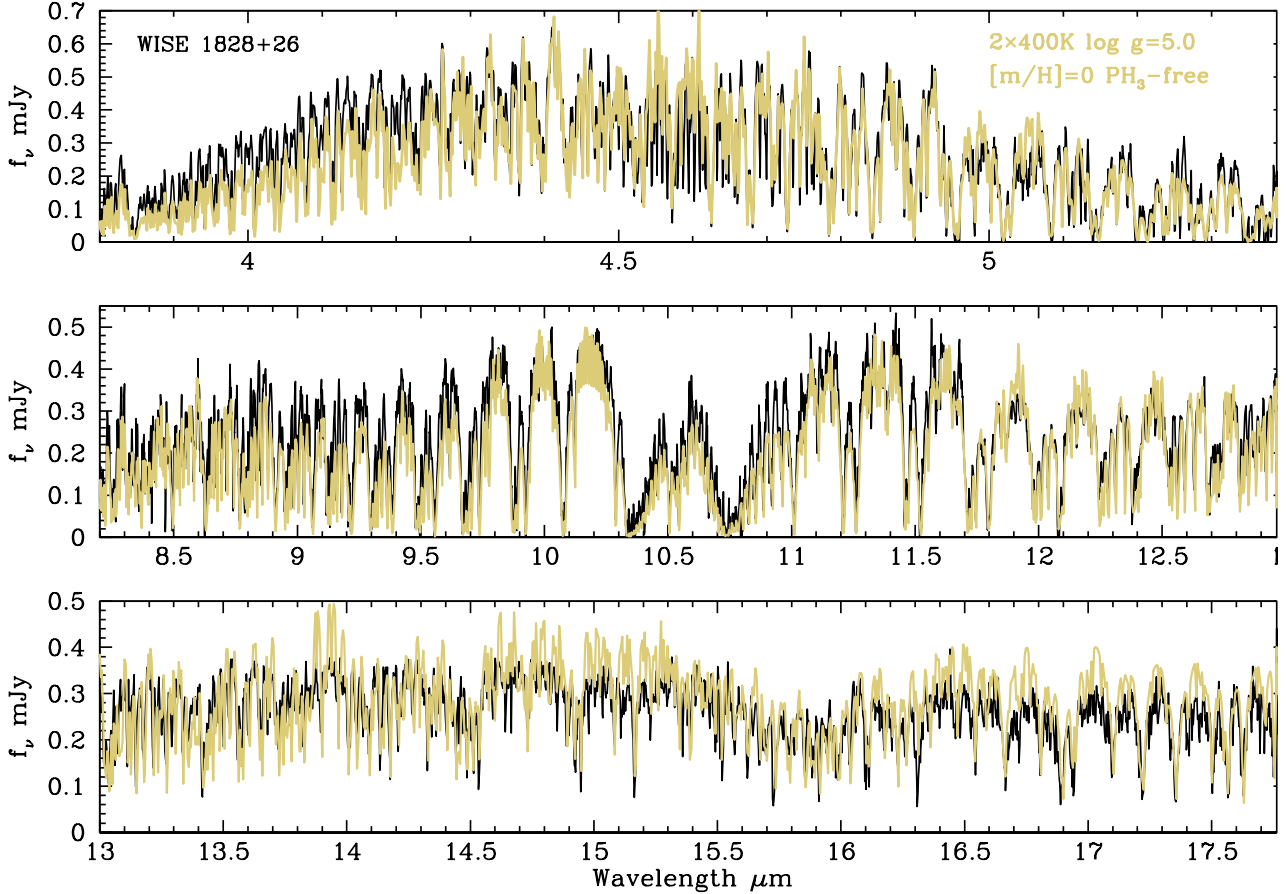


**Figure 6.** A more detailed comparison of the *JWST* NIRSpec and MIRI data for WISEPA J182831.08+265037.8 (Barrado et al. 2023; Lew et al. 2024) and the synthetic ATMO 2020++ spectrum for the adopted solution for the system, an identical pair of 400 K  $\log g = 5.0$  solar metallicity dwarfs. Absorption features due to (primarily) CO, CO<sub>2</sub>, CH<sub>4</sub>, H<sub>2</sub>O, and NH<sub>3</sub> are identified in Figure 5 of Lew et al. (2024) and Figure 1 of Barrado et al. (2023).

typical average deviation is  $5\sigma$ , although both fits underestimate the flux at  $3.8 \lesssim \lambda \mu\text{m} \lesssim 4.2$  (Figure 5). Most likely this is due to the known remaining deficiencies in the models, which calculate too low a flux around the  $3.3 \mu\text{m}$  CH<sub>4</sub> absorption band (see discussion in Leggett et al. 2021). The two solutions have similar GF values, with a slight preference for the solar metallicity, higher gravity, solution (for example, for  $4.3 \leq \lambda \mu\text{m} \leq 17.9$  the average deviation is  $5.1\sigma$  for solution (1) and  $5.7\sigma$  for solution (2)). Figure 6 shows a more detailed comparison using solution (1). The near-infrared fit (seen in the inset panel of Figure 5), could be improved by tuning  $\gamma$  and  $P_{(\gamma, \text{max})}$  to adjust the pressure-temperature profile in the interior of the atmosphere, where these fluxes originate (Figure 6 of Leggett et al. 2021).

Figure 5 also shows comparisons of the data to synthetic ATMO 2020++ spectra with atmospheric parameters similar to those found in model analyses of the NIRSpec and MIRI spectra separately, by Lew et al. (2024) and Barrado et al. (2023).

- Lew et al. (2024) used Elf-Owl models (Mukherjee et al. 2022) with the  $2.9 \lesssim \lambda \mu\text{m} \lesssim 5.1$  NIRSpec data to determine  $T_{\text{eff}} = 425 \text{ K}$ ,  $\log g = 4.4$ , and  $[\text{m}/\text{H}] = -0.6$ . The bottom panel of



Figure 5 shows the ATMO 2020++ spectrum for similar parameters, created by interpolating the 400 K and 450 K  $\log g = 4.5$   $[\text{m}/\text{H}] = -0.5$  grid models (olive lines). The agreement with the observed  $4.0 \lesssim \lambda \mu\text{m} \lesssim 18$  spectrum could be made acceptable with an increase in the scaling factor of  $\approx 25\%$ , however this would increase the discrepancy in the near-infrared where the model flux is a factor of  $\sim 3$  too bright at  $J$  and  $H$ . Improving the agreement in the near-infrared would require a larger deviation from an adiabatic pressure-temperature relationship in order to cool the interior atmosphere.

- Barrado et al. (2023) used ATMO 2020++ models (Leggett et al. 2021; Leggett & Tremblin 2023; Meisner et al. 2023) with the  $5.0 \lesssim \lambda \mu\text{m} \lesssim 18$  MIRI data to determine  $T_{\text{eff}} = 400 \text{ K}$ ,  $\log g = 4.0$ , and  $[\text{m}/\text{H}] = 0.0$  (green line in Figure 5). The bottom panel of Figure 5 shows that while the agreement with the MIRI data is very good, the flux in the  $4.5 \mu\text{m}$  region is approximately half what is observed. That is, adoption of a lower gravity increases the CO and CO<sub>2</sub> absorption at  $4.7 \mu\text{m}$  and  $4.25 \mu\text{m}$  and produces a spectrum that does not reproduce the NIRSpec data; the W2 – W3 color is too red, as also demonstrated in Figure 4. Furthermore, the discrepancy in the near-infrared is around a factor of 5 (Figure 5). Barrado et al. also use the ARCiS framework (Ormel & Min 2019) for a self-consistent atmospheric analysis of the MIRI data, and determine  $T_{\text{eff}} = 500 \text{ K}$  and  $\log g = 5.0$ . Figure 4 indicates that a brown dwarf this warm will be more than ten times brighter than observed, at near-infrared wavelengths.

Lew et al. (2024) and Barrado et al. (2023) also explore retrieval analyses. The Lew et al. CHIMERA (Line et al. 2014) retrieval result of  $T_{\text{eff}} = 530 \text{ K}$  and  $\log g = 5.2$ , like the Barrado et al. ARCiS self-consistent result, will be incompatible with the observed near-infrared flux (Figure 4). Barrado et al. (2023) use ARCiS (Ormel & Min 2019), Brewster (Bunningham et al. 2017), and petitRADTRANS (Mollière et al. 2019) for their retrieval analyses of the MIRI data. They find solar metallicity solutions with  $T_{\text{eff}}$  values between 350 K and 400 K, and  $\log g$  values between 3.8 and 4.7; they also find a metal-poor solution with a very low gravity of 3.4 dex. The ATMO 2020++ models indicate that the lower gravity solutions will be inconsistent with the NIRSpec data, as shown spectroscopically in the bottom panel of Figure 5, and photometrically in Figure 4. The higher gravity solutions are consistent with our results, and the Barrado et al. (2023) radii are consistent with evolutionary models if the source is an unresolved binary.

In summary, broad wavelength coverage is required for reliable analyses of brown dwarf spectra. Taken separately, the near-infrared region, the  $4.5 \mu\text{m}$  region, and the  $12 \mu\text{m}$  region, can each indicate atmospheric properties that are excluded by data at other wavelengths. While our preferred ATMO 2020++ solutions show some discrepancies at  $\lambda \approx 1.6 \mu\text{m}$  and  $\lambda \approx 4.0 \mu\text{m}$  (Figure 5, top two panels), they provide an excellent fit across the spectral regions where significant flux is emitted (Figure 6).

Adopting a  $T_{\text{eff}} = 400 \text{ K}$  and  $\log g = 5.0$  binary solution, evolutionary models then imply an age of 8 to 15 Gyr, corresponding to masses of 20 to 30  $M_{\text{Jup}}$  respectively, for each component (Marley et al. 2021). The tangential velocity of  $48 \text{ km s}^{-1}$  suggests thin disk membership (Figure 31 of Dupuy & Liu 2012), and so an age at the younger end of this range, and a mass at the smaller end, is more likely. This is a tight system – De Furio et al. (2023) find that the separation must be smaller than 0.5 au, or around 1000 brown dwarf radii. An order-of-magnitude estimate by Lew et al. (2024), based on the radial velocity, suggests an even smaller separation of 20 Jupiter radii.

This enigmatic source therefore seems to be revealing itself as a high gravity, massive, tightly bound, brown dwarf binary. The analysis here also supports the use of the W2 – W3 color (or similar passbands) as a gravity indicator.

#### 4. APPLICATION TO *JWST* IMAGING

Figure 7 shows a color-magnitude diagram using *JWST* filters, similar to the top panel of Figure 4. Spectral coverage of each of these wide bandpasses is illustrated in Figure 2. The F1130W filter was not considered as the bandpass is narrower and the sensitivity is reduced.

We synthesized F444W, F1000W, F1280W, and F1500W magnitudes for WISE 1828 using the NIRSpec and MIRI spectra published by [Lew et al. \(2024\)](#) and [Barrado et al. \(2023\)](#). The MIRI spectrum does not cover the entire F1800W bandpass. We determined: F444W = 14.45, F1000W = 13.11, F1280W = 12.45, and F1500W = 12.03. The uncertainty is dominated by the absolute flux uncertainty in the spectra, currently estimated to be around 5% <sup>2</sup>.

Also shown in Figure 7 are F444W, F1000W, F1500W, and F1800W colors for 22 T and Y dwarfs from [Beiler et al. \(2024, their Tables 1 and 9\)](#). The F444W magnitudes are synthesized from NIRSpec spectra, while F1000W, F1500W, and F1800W are from MIRI imaging observations. The Beiler et al. sample of brown dwarfs appears to be typical of the local disk, with the T dwarfs ( $T_{\text{eff}} \gtrsim 500$  K) having  $\log g$  values of 4.5 to 5.0, and the Y dwarfs ( $T_{\text{eff}} \lesssim 500$  K) having  $\log g$  values of 4.0 to 4.5, both corresponding to ages of a few Gyr ([Marley et al. 2021, their Figure 10](#)). While there are no extremely low-gravity sources in the sample, one source is likely to be high gravity and metal-poor: WISE J043052.92+463331. This T8 dwarf has the bluest F444W – F1000W color in the [Beiler et al. \(2024\)](#) sample and has been flagged as abnormally red in  $H$ –W2, and faint in  $H$  by [Best et al. \(2021\)](#).

The models are in excellent agreement with the observations — both in terms of the colors and the  $T_{\text{eff}}$  values, which were determined by [Beiler et al. \(2024\)](#) using the observed bolometric luminosity. Figure 7 shows that the shorter wavelength colors – F444W – F1000W and F444W – F1280 – are more sensitive to gravity than the longer wavelength colors, however F444W – F1500W and F444W – F1800W continue to increase with decreasing  $T_{\text{eff}}$ , making them useful for temperature estimates in the absence of a distance measurement. To ease comparisons using different 4.5  $\mu\text{m}$  filter bandpasses, [Leggett & Tremblin \(2023, their Figure 6 and Table 3\)](#) provide transformations determined from synthetic spectra; the differences are relatively small – around 0.2 magnitudes for late-T and Y dwarfs.

#### 5. CONCLUSIONS

Separating metallicity and surface gravity effects in near-infrared spectra of cool brown dwarfs has been a long-standing challenge (e.g. [Burgasser et al. 2006a](#); [Liu et al. 2007](#); [Leggett et al. 2017](#)). Inspired by clear trends seen at  $4 \lesssim \lambda \mu\text{m} \lesssim 15$  in early fits of *JWST* Y dwarf spectra ([Leggett & Tremblin 2024](#)), we explored the sensitivity of late-T and Y dwarf *WISE* W2 and W3 colors to  $T_{\text{eff}}$ ,  $[\text{m}/\text{H}]$ , and  $\log g$ , after reviewing and updating the W3 magnitudes of 82 objects (Section 2). We use PH<sub>3</sub>-free ATMO 2020++ models which have been shown to reproduce *JWST* spectroscopic

<sup>2</sup> <https://jwst-docs.stsci.edu/jwst-calibration-status/jwst-absolute-flux-calibration#gsc.tab=0>

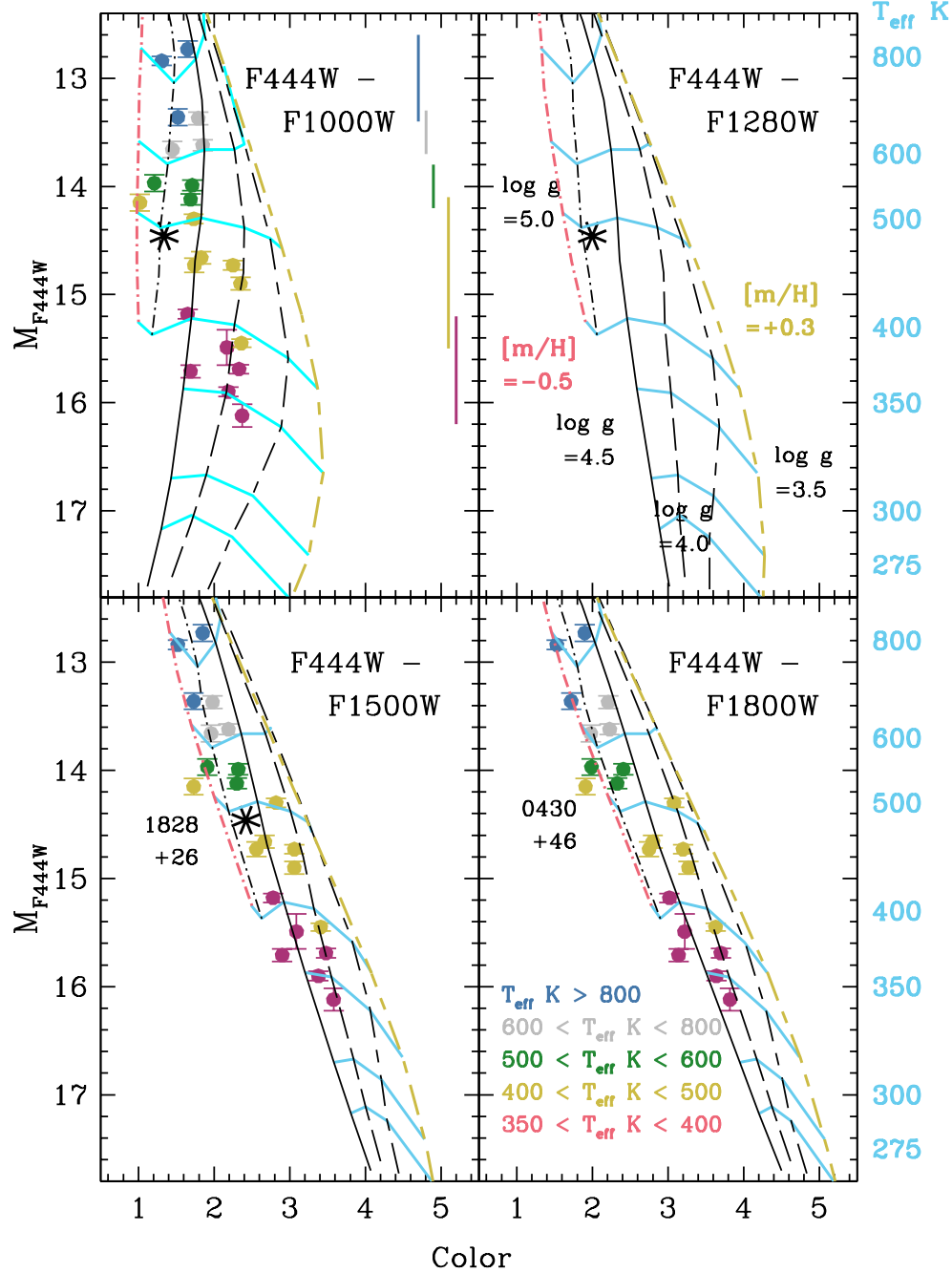


**Figure 7.** Color-magnitude diagram for late T and Y dwarfs, using *JWST* filters. Filled circles represent F444W, F1000W, F1500W and F1800W colors from Beiler et al. (2024). The symbol color indicates the luminosity-based  $T_{\text{eff}}$  value determined by Beiler et al., see the legend in the lower right. Colored bars in the upper left illustrate the range in  $M_{\text{F444W}}$  for each temperature group. The black asterisk represents WISE 1828, using F444W, F1000W, F1280W and F1500W colors synthesized here from *JWST* spectra. Vertical lines are ATMO 2020++ PH<sub>3</sub>-free sequences, with cyan lines showing isotherms for the model  $T_{\text{eff}}$  on the right axes. The black lines are  $\log g = 3.5, 4.0, 4.5,$  and  $5.0$  from right to left. The red line is a  $\log g = 5.0$  sequence with  $[m/H] = -0.5$  and the yellow line is a  $\log g = 3.5$  sequence with  $[m/H] = +0.3$ . The source with the bluest F444W – F1000W color is WISE J043052.92+463331.

observations of late-T and Y dwarfs over a broad wavelength range of  $1 \lesssim \lambda \mu\text{m} \lesssim 14$  (Leggett & Tremblin 2023, 2024; Tu et al. 2024). The  $T_{\text{eff}}$  values determined using ATMO 2020++ synthetic spectra are in good agreement with values determined semi-empirically by Beiler et al. (2023) using bolometric luminosity arguments (Figure 7). Furthermore, the  $T_{\text{eff}}$  and  $\log g$  values are consistent with evolutionary models (e.g. Marley et al. 2021), assuming this local sample of brown dwarfs has an age range of around 0.5 Gyr to 6 Gyr (Dupuy & Liu 2017; Kirkpatrick et al. 2019; Best et al. 2024).

We find that for  $T_{\text{eff}} \lesssim 600$  K the W2 – W3 color becomes very sensitive to gravity, while being only mildly sensitive to metallicity (Figures 4 and 7). Other observations and analyses support this conclusion:

- We identify ten very red, likely low-gravity, low-mass young brown dwarfs or exoplanets, listed in Table 3. Two of these are companions to main sequence stars and previous analyses (Zhang et al. 2021; Rothermich et al. 2024) have found the systems to be young (100 – 800 Myr). Previous near-infrared spectral analysis of a third source supports the low gravity, mass, and age ( $\log g \approx 3.7$ , Zhang et al. (2021); Zalesky et al. (2022)). Two additional sources have kinematics indicative of a young age. Followup observations are required to confirm the young and low-mass nature of these objects: CWISE J004143.77–401929.9, CWISEP J010650.61+225159.1, CWISE J104053.42–355029.7, ULAS J115229.67+035927.2, and WISE J223204.50-573010.5 (Section 3.3).
- The sources with the bluest W2 – W3 colors, which the models show to be indicative of high gravity and metal paucity, are known metal-poor T dwarfs, and are likely to be around 8 Gyr old with masses around  $35 M_{\text{Jup}}$  (Section 3.4).
- The revised W3 magnitude for the Y dwarf WISEPA J182831.08+265037.8 places it along the high gravity W2 – W3 sequence in Figure 4. We find excellent agreement with the observed 4 to 18  $\mu\text{m}$  *JWST* spectra (Barrado et al. 2023; Lew et al. 2024) if the system is a pair of similar cold brown dwarfs with  $T_{\text{eff}}$  350 K to 400 K, surface gravities  $g$  in the range  $\log g$  4.5 to 5.0 dex, and a solar or slightly sub-solar metallicity. Evolutionary models then imply an age around 8 Gyr and a mass  $\sim 20 M_{\text{Jup}}$  for each component. The separation is less than 1000 radii based on unresolved *JWST* images (De Furio et al. 2023).

Other evidence therefore supports the model trends shown in Figure 4, illustrating the power of a color which measures the slope of the energy distribution from  $\lambda \sim 5 \mu\text{m}$  to  $\lambda \sim 10 \mu\text{m}$ .

The *WISE* W3 magnitude is difficult to measure to better than around 20% for sources with W3  $\approx 13$ , due to the large pixels of the camera and the high and spatially-variable background. MIRI imaging with *JWST* offers the opportunity to reach a higher precision and fainter sources. Beiler et al. (2024) determine accurate mid-infrared colors ( $\pm 3\%$ ) and  $T_{\text{eff}}$  values ( $\pm 4\%$  to  $7\%$ ) for a sample of 22 T and Y brown dwarfs as faint as 14th magnitude at  $\lambda = 10 \mu\text{m}$ . Figure 7 shows that the ATMO 2020++ models are in excellent agreement with the data, illustrating the potential of combining *JWST* data with these models. For example, the models demonstrate that the Beiler et al. sample has a range in surface gravity which corresponds to a local disk sample aged 0.5 Gyr to 6 Gyr (using the evolutionary models of Marley et al. 2021), and a small range in metallicity, typical of the local solar neighborhood (e.g. Hinkel et al. 2014).

Future mid-infrared missions with sufficient sensitivity at  $4 \lesssim \lambda \mu\text{m} \lesssim 15$  will be able to identify old or very metal-poor brown dwarfs in the solar neighborhood, as well as exoplanets and planetary-mass free-floating brown dwarfs. The Near-Earth Object Surveyor Mission, scheduled for launch in 2027 or 2028<sup>3</sup> is designed to detect 200 K to 300 K objects in filters centered near 4.6  $\mu\text{m}$  and 8  $\mu\text{m}$  (Mainzer et al. 2023). The 8  $\mu\text{m}$  sensitivity of  $\sim 5$  mJy, illustrated in Mainzer et al. (2023), suggests that a detection in both filters is limited to young low-mass 350 K – 400 K brown dwarfs which are closer than  $\sim 4$  pc, based on the ATMO 2020++ models. Current space density estimates of Y dwarfs (Kirkpatrick et al. 2021a; Best et al. 2024) then suggest that zero to 1 dwarf will be detected. However these estimates are very uncertain and the mission remains of great interest for brown dwarf and exoplanet science, as well as solar system science.

The Appendix provides the photometric data compilation used in this work, which is described in Section 2. The model spectra and colors are publicly available at <https://opendata.erc-atmo.eu>, under the heading “ATMO 2020++ grid without PH3, Leggett & Tremblin (2024)”.

We are very grateful to the referee, whose comments significantly improved this paper.

We are beyond grateful to the many engineers and scientists who made the NIRSpec and MIRI instruments, and the *JWST*, the success that they are.

This research has made use of the NASA/IPAC Infrared Science Archive, which is funded by the National Aeronautics and Space Administration and operated by the California Institute of Technology.

## APPENDIX

### A. PHOTOMETRY COMPILATION

Table 4 presents a compilation of photometry.

<sup>3</sup> <https://neos.arizona.edu/>

Table 4. Compilation of Photometric Measurements for T- and Y-Type Brown Dwarfs

| Survey | Discovery RA         | Decl.     | Sp.  | M     | -m    | Y     | J     | H             | K             | L'            | [3.6]         | [4.5]         | W1            | W2            | W3            | $e_{Mm}$      | $e_Y$         | $e_J$          | $e_H$          | $e_K$          | $e_{L'}$       | $e_{3.6}$      | $e_{4.5}$      | $e_{W1}$       | $e_{W2}$       | $e_{W3}$         | References     | Parallax         | Near-IR        | Sp. Type         | Discovery      | Sp. Type         | References     |
|--------|----------------------|-----------|------|-------|-------|-------|-------|---------------|---------------|---------------|---------------|---------------|---------------|---------------|---------------|---------------|---------------|----------------|----------------|----------------|----------------|----------------|----------------|----------------|----------------|------------------|----------------|------------------|----------------|------------------|----------------|------------------|----------------|
| Name   | hhmmss.ss ± dddmss.s |           | Type | mag   |       |       |       |               |               |               |               |               |               |               |               |               |               |                |                |                |                |                |                |                |                |                  | Discovery      | Sp. Type         | References     |                  |                |                  |                |
| CWISEP | 000229.93            | +635217.0 | 7.5  | 17.35 | 15.69 | 0.25  | 0.06  | Meisner_2020b | Meisner_2020b | Meisner_2020b | Meisner_2020b | Meisner_2020b | Meisner_2020b | Meisner_2020b | Meisner_2020b | Meisner_2020b | Meisner_2020b | Meisner_2020b  | Meisner_2020b  | Meisner_2020b  | Meisner_2020b  | Meisner_2020b  | Meisner_2020b  | Meisner_2020b  | Meisner_2020b  | Meisner_2020b    | Meisner_2020b  | Meisner_2020b    | Meisner_2020b  | Meisner_2020b    | Meisner_2020b  | Meisner_2020b    |                |
| WISE   | 000517.48            | +373720.5 | 9.0  | 0.52  | 18.48 | 17.59 | 17.98 | 17.99         | 14.43         | 15.43         | 13.28         | 16.76         | 13.29         | 11.79         | 0.04          | 0.02          | 0.02          | 0.08           | 0.03           | 0.10           | 0.04           | 0.04           | 0.09           | 0.03           | 0.24           | Kirkpatrick_2019 | Leggett_2015   | Kirkpatrick_2019 | Leggett_2015   | Kirkpatrick_2019 | Leggett_2015   | Kirkpatrick_2019 |                |
| CWISEP | 001146.07            | -471306.8 | 8.5  | 19.28 | 19.69 | 0.07  | 0.20  | Mace_2013a    | Mace_2013a    | Mace_2013a    | Mace_2013a    | Mace_2013a    | Mace_2013a    | Mace_2013a    | Mace_2013a    | Mace_2013a    | Mace_2013a    | Mace_2013a     | Mace_2013a     | Mace_2013a     | Mace_2013a     | Mace_2013a     | Mace_2013a     | Mace_2013a     | Mace_2013a     | Mace_2013a       | Mace_2013a     | Mace_2013a       | Mace_2013a     | Mace_2013a       | Mace_2013a     | Mace_2013a       | Mace_2013a     |
| WISE   | 001354.39            | +063448.2 | 8.0  | 20.56 | 19.54 | 19.98 | 20.79 | 17.45         | 15.16         | 15.23         | 0.04          | 0.03          | 0.04          | 0.10          | 0.03          | 0.03          | 0.09          | Pinfield_2014a | Pinfield_2014a | Pinfield_2014a | Pinfield_2014a | Pinfield_2014a | Pinfield_2014a | Pinfield_2014a | Pinfield_2014a | Pinfield_2014a   | Pinfield_2014a | Pinfield_2014a   | Pinfield_2014a | Pinfield_2014a   | Pinfield_2014a | Pinfield_2014a   | Pinfield_2014a |
| WISEA  | 001449.96            | +795116.1 | 8.0  | 20.32 | 19.36 | 17.76 | 15.88 | 18.72         | 16.00         | 13.69         | 0.10          | 0.10          | 0.04          | 0.02          | 0.28          | 0.06          | 0.40          | Bardalez_2020  | Bardalez_2020  | Bardalez_2020  | Bardalez_2020  | Bardalez_2020  | Bardalez_2020  | Bardalez_2020  | Bardalez_2020  | Bardalez_2020    | Bardalez_2020  | Bardalez_2020    | Bardalez_2020  | Bardalez_2020    | Bardalez_2020  | Bardalez_2020    | Bardalez_2020  |

NOTE—Table 4 is published in its entirety in the machine-readable format. A portion is shown here for guidance regarding its form and content.

**References**—2MASS – Skrutskie et al. (2006); Albert\_2011 – Albert et al. (2011); Artigau\_2010 – Artigau et al. (2010); Bardalez\_2020 – Bardalez Gagliuffi et al. (2020); Beichman\_2014 – Beichman et al. (2014); Beiler\_2024 – Beiler et al. (2024); Best\_2015 – Best et al. (2015); Best\_2020 – Best et al. (2020); Best\_2021 – Best et al. (2021); Brooks\_2022 – Brooks et al. (2022); Burgasser\_1999 – Burgasser et al. (1999); Burgasser\_2000 – Burgasser et al. (2000); Burgasser\_2002 – Burgasser et al. (2002); Burgasser\_2003 – Burgasser et al. (2003); Burgasser\_2004 – Burgasser et al. (2004); Burgasser\_2006 – Burgasser et al. (2006b); Burgasser\_2008 – Burgasser et al. (2008); Burgasser\_2010 – Burgasser et al. (2010); Burgasser\_2012 – Burgasser et al. (2012); Burningham\_2008 – Burningham et al. (2008); Burningham\_2009 – Burningham et al. (2009); Burningham\_2010a – Burningham et al. (2010); Burningham\_2010b – Burningham et al. (2010); Burningham\_2011 – Burningham et al. (2011); Burningham\_2013 – Burningham et al. (2013); Chiu\_2006 – Chiu et al. (2006); Cushing\_2011 – Cushing et al. (2011); Cushing\_2014 – Cushing et al. (2014); Cushing\_2016 – Cushing et al. (2016); Delorme\_2008 – Delorme et al. (2008); Delorme\_2010 – Delorme et al. (2010); Dupuy\_2012 – Dupuy & Liu (2012); Dupuy\_2015 – Dupuy et al. (2015); Faherty\_2012 – Faherty et al. (2012); Faherty\_2020 – Faherty et al. (2020); Gaia – Gaia Collaboration et al. (2018); Geballe\_2001 – Geballe et al. (2001); Gelino\_2011 – Gelino et al. (2011); Goldman\_2010 – Goldman et al. (2010); Golimowski\_2004 – Golimowski et al. (2004); Greco\_2019 – Greco et al. (2019); Griffith\_2012 – Griffith et al. (2012); Kirkpatrick\_2011 – Kirkpatrick et al. (2011); Kirkpatrick\_2012 – Kirkpatrick et al. (2012); Kirkpatrick\_2013 – Kirkpatrick et al. (2013); Kirkpatrick\_2019 – Kirkpatrick et al. (2019); Kirkpatrick\_2021a – Kirkpatrick et al. (2021a); Kirkpatrick\_2021b – Kirkpatrick et al. (2021b); Knapp\_2004 – Knapp et al. (2004); Kota\_2022 – Kota et al. (2022); Leggett\_2002 – Leggett et al. (2002); Leggett\_2009 – Leggett et al. (2009); Leggett\_2010 – Leggett et al. (2010); Leggett\_2012 – Leggett et al. (2012); Leggett\_2013 – Leggett et al. (2013); Leggett\_2014 – Leggett et al. (2014); Leggett\_2015 – Leggett et al. (2015); Leggett\_2017 – Leggett et al. (2017); Leggett\_2019 – Leggett et al. (2019); Leggett\_2021 – Leggett et al. (2021); Liu\_2011 – Liu et al. (2011); Liu\_2012 – Liu et al. (2012); Lodieu\_2007 – Lodieu et al. (2007); Lodieu\_2009 – Lodieu et al. (2009); Lodieu\_2012 – Lodieu et al. (2012); Lodieu\_2022 – Lodieu et al. (2022); Looper\_2007 – Looper et al. (2007); Lucas\_2010 – Lucas et al. (2010); Luhman\_2011 – Luhman et al. (2011); Luhman\_2012 – Luhman et al. (2012); Luhman\_2014 – Luhman et al. (2014); Mace\_2013a – Mace et al. (2013a); Mace\_2013b – Mace et al. (2013b); Mainzer\_2011 – Mainzer et al. (2011); Manjavacas\_2013 – Manjavacas et al. (2013); Marocco\_2010 – Marocco et al. (2010); Marocco\_2020 – Marocco et al. (2020); Martin\_2018 – Martin et al. (2018); Meisner\_2020a – Meisner et al. (2020a); Meisner\_2020b – Meisner et al. (2020b); Meisner\_2021 – Meisner et al. (2021); Meisner\_2023 – Meisner et al. (2023); Meisner\_2024 – Meisner et al. (2024); Murray\_2011 – Murray et al. (2011); Patten\_2006 – Patten et al. (2006); Pinfield\_Gronadzki\_2014 – Pinfield, P. and Gronadzki, M. private communication 2014; Pinfield\_2008 – Pinfield et al. (2008); Pinfield\_2012 – Pinfield et al. (2012); Pinfield\_2014a – Pinfield et al. (2014a); Pinfield\_2014b – Pinfield et al. (2014b); Robbins\_2023 – Robbins et al. (2023); Rothermich\_2024 – Rothermich et al. (2024); Schneider\_2015 – Schneider et al. (2015); Schneider\_2020 – Schneider et al. (2020); Schneider\_2021 – Schneider et al. (2021); Scholz\_2010a – Scholz (2010a); Scholz\_2010b – Scholz (2010b); Scholz\_2011 – Scholz et al. (2011); Scholz\_2012 – Scholz et al. (2012); Smart\_2010 – Smart et al. (2010); Strauss\_1999 – Strauss et al. (1999); Subasavage\_2009 – Subasavage et al. (2009); Thompson\_2013 – Thompson et al. (2013); Tinney\_2003 – Tinney et al. (2003); Tinney\_2005 – Tinney et al. (2005); Tinney\_2012 – Tinney et al. (2012); Tinney\_2014 – Tinney et al. (2014); Tinney\_2018 – Tinney et al. (2018); Tsvetanov\_2000 – Tsvetanov et al. (2000); TW – This Work; UKIDSS – Lawrence et al. (2007); VISTA – Sutherland et al. (2015); Vrba\_2004 – Vrba et al. (2004); Warren\_2007 – Warren et al. (2007); Wright\_2013 – Wright et al. (2013)



## REFERENCES

- Ackerman, A. S., & Marley, M. S. 2001, *ApJ*, 556, 872, doi: [10.1086/321540](https://doi.org/10.1086/321540)
- Albert, L., Artigau, É., Delorme, P., et al. 2011, *AJ*, 141, 203, doi: [10.1088/0004-6256/141/6/203](https://doi.org/10.1088/0004-6256/141/6/203)
- Artigau, É., Radigan, J., Folkes, S., et al. 2010, *ApJL*, 718, L38, doi: [10.1088/2041-8205/718/1/L38](https://doi.org/10.1088/2041-8205/718/1/L38)
- Bardalez Gagliuffi, D. C., Faherty, J. K., Schneider, A. C., et al. 2020, *ApJ*, 895, 145, doi: [10.3847/1538-4357/ab8d25](https://doi.org/10.3847/1538-4357/ab8d25)
- Barrado, D., Mollière, P., Patapis, P., et al. 2023, *Nature*, 624, 263, doi: [10.1038/s41586-023-06813-y](https://doi.org/10.1038/s41586-023-06813-y)
- Beichman, C., Gelino, C. R., Kirkpatrick, J. D., et al. 2013, *ApJ*, 764, 101, doi: [10.1088/0004-637X/764/1/101](https://doi.org/10.1088/0004-637X/764/1/101)
- . 2014, *ApJ*, 783, 68, doi: [10.1088/0004-637X/783/2/68](https://doi.org/10.1088/0004-637X/783/2/68)
- Beiler, S. A., Cushing, M. C., Kirkpatrick, J. D., et al. 2023, *ApJL*, 951, L48, doi: [10.3847/2041-8213/ace32c](https://doi.org/10.3847/2041-8213/ace32c)
- . 2024, *ApJ*, 973, 107, doi: [10.3847/1538-4357/ad6301](https://doi.org/10.3847/1538-4357/ad6301)
- Best, W. M. J., Liu, M. C., Magnier, E. A., & Dupuy, T. J. 2020, *AJ*, 159, 257, doi: [10.3847/1538-3881/ab84f4](https://doi.org/10.3847/1538-3881/ab84f4)
- . 2021, *AJ*, 161, 42, doi: [10.3847/1538-3881/abc893](https://doi.org/10.3847/1538-3881/abc893)
- Best, W. M. J., Sanghi, A., Liu, M. C., Magnier, E. A., & Dupuy, T. J. 2024, *ApJ*, 967, 115, doi: [10.3847/1538-4357/ad39ef](https://doi.org/10.3847/1538-4357/ad39ef)
- Best, W. M. J., Liu, M. C., Magnier, E. A., et al. 2015, *ApJ*, 814, 118, doi: [10.1088/0004-637X/814/2/118](https://doi.org/10.1088/0004-637X/814/2/118)
- Brooks, H., Kirkpatrick, J. D., Caselden, D., et al. 2022, *AJ*, 163, 47, doi: [10.3847/1538-3881/ac3a0a](https://doi.org/10.3847/1538-3881/ac3a0a)
- Burgasser, A. J., Burrows, A., & Kirkpatrick, J. D. 2006a, *ApJ*, 639, 1095, doi: [10.1086/499344](https://doi.org/10.1086/499344)
- Burgasser, A. J., Cruz, K. L., Cushing, M., et al. 2010, *ApJ*, 710, 1142, doi: [10.1088/0004-637X/710/2/1142](https://doi.org/10.1088/0004-637X/710/2/1142)
- Burgasser, A. J., Geballe, T. R., Leggett, S. K., Kirkpatrick, J. D., & Golimowski, D. A. 2006b, *ApJ*, 637, 1067, doi: [10.1086/498563](https://doi.org/10.1086/498563)
- Burgasser, A. J., Gelino, C. R., Cushing, M. C., & Kirkpatrick, J. D. 2012, *ApJ*, 745, 26, doi: [10.1088/0004-637X/745/1/26](https://doi.org/10.1088/0004-637X/745/1/26)
- Burgasser, A. J., McElwain, M. W., & Kirkpatrick, J. D. 2003, *AJ*, 126, 2487, doi: [10.1086/378608](https://doi.org/10.1086/378608)
- Burgasser, A. J., McElwain, M. W., Kirkpatrick, J. D., et al. 2004, *AJ*, 127, 2856, doi: [10.1086/383549](https://doi.org/10.1086/383549)
- Burgasser, A. J., Tinney, C. G., Cushing, M. C., et al. 2008, *ApJL*, 689, L53, doi: [10.1086/595747](https://doi.org/10.1086/595747)
- Burgasser, A. J., Kirkpatrick, J. D., Brown, M. E., et al. 1999, *ApJL*, 522, L65, doi: [10.1086/312221](https://doi.org/10.1086/312221)
- Burgasser, A. J., Kirkpatrick, J. D., Cutri, R. M., et al. 2000, *ApJL*, 531, L57, doi: [10.1086/312522](https://doi.org/10.1086/312522)
- Burgasser, A. J., Kirkpatrick, J. D., Brown, M. E., et al. 2002, *ApJ*, 564, 421, doi: [10.1086/324033](https://doi.org/10.1086/324033)
- Burningham, B., Marley, M. S., Line, M. R., et al. 2017, *MNRAS*, 470, 1177, doi: [10.1093/mnras/stx1246](https://doi.org/10.1093/mnras/stx1246)
- Burningham, B., Pinfield, D. J., Leggett, S. K., et al. 2008, *MNRAS*, 391, 320, doi: [10.1111/j.1365-2966.2008.13885.x](https://doi.org/10.1111/j.1365-2966.2008.13885.x)
- . 2009, *MNRAS*, 395, 1237, doi: [10.1111/j.1365-2966.2009.14620.x](https://doi.org/10.1111/j.1365-2966.2009.14620.x)
- Burningham, B., Leggett, S. K., Lucas, P. W., et al. 2010, *MNRAS*, 404, 1952, doi: [10.1111/j.1365-2966.2010.16411.x](https://doi.org/10.1111/j.1365-2966.2010.16411.x)
- Burningham, B., Pinfield, D. J., Lucas, P. W., et al. 2010, *MNRAS*, 406, 1885, doi: [10.1111/j.1365-2966.2010.16800.x](https://doi.org/10.1111/j.1365-2966.2010.16800.x)
- Burningham, B., Lucas, P. W., Leggett, S. K., et al. 2011, *MNRAS*, 414, L90, doi: [10.1111/j.1745-3933.2011.01062.x](https://doi.org/10.1111/j.1745-3933.2011.01062.x)
- Burningham, B., Cardoso, C. V., Smith, L., et al. 2013, *MNRAS*, 433, 457, doi: [10.1093/mnras/stt740](https://doi.org/10.1093/mnras/stt740)
- Burrows, A., & Liebert, J. 1993, *Reviews of Modern Physics*, 65, 301, doi: [10.1103/RevModPhys.65.301](https://doi.org/10.1103/RevModPhys.65.301)
- Burrows, A., Sudarsky, D., & Lunine, J. I. 2003, *ApJ*, 596, 587, doi: [10.1086/377709](https://doi.org/10.1086/377709)
- Chiu, K., Fan, X., Leggett, S. K., et al. 2006, *AJ*, 131, 2722, doi: [10.1086/501431](https://doi.org/10.1086/501431)
- Cushing, M. C., Kirkpatrick, J. D., Gelino, C. R., et al. 2014, *AJ*, 147, 113, doi: [10.1088/0004-6256/147/5/113](https://doi.org/10.1088/0004-6256/147/5/113)

- . 2011, *ApJ*, 743, 50,  
doi: [10.1088/0004-637X/743/1/50](https://doi.org/10.1088/0004-637X/743/1/50)
- Cushing, M. C., Hardegree-Ullman, K. K., Trucks, J. L., et al. 2016, *ApJ*, 823, 152,  
doi: [10.3847/0004-637X/823/2/152](https://doi.org/10.3847/0004-637X/823/2/152)
- Cushing, M. C., Schneider, A. C., Kirkpatrick, J. D., et al. 2021, *ApJ*, 920, 20,  
doi: [10.3847/1538-4357/ac12cb](https://doi.org/10.3847/1538-4357/ac12cb)
- De Furio, M., Lew, B., Beichman, C., et al. 2023, *ApJ*, 948, 92, doi: [10.3847/1538-4357/acbf1e](https://doi.org/10.3847/1538-4357/acbf1e)
- Delorme, P., Delfosse, X., Albert, L., et al. 2008, *A&A*, 482, 961,  
doi: [10.1051/0004-6361:20079317](https://doi.org/10.1051/0004-6361:20079317)
- Delorme, P., Albert, L., Forveille, T., et al. 2010, *A&A*, 518, A39,  
doi: [10.1051/0004-6361/201014277](https://doi.org/10.1051/0004-6361/201014277)
- Dupuy, T. J., & Kraus, A. L. 2013, *Science*, 341, 1492, doi: [10.1126/science.1241917](https://doi.org/10.1126/science.1241917)
- Dupuy, T. J., & Liu, M. C. 2012, *ApJS*, 201, 19,  
doi: [10.1088/0067-0049/201/2/19](https://doi.org/10.1088/0067-0049/201/2/19)
- . 2017, *ApJS*, 231, 15,  
doi: [10.3847/1538-4365/aa5e4c](https://doi.org/10.3847/1538-4365/aa5e4c)
- Dupuy, T. J., Liu, M. C., & Leggett, S. K. 2015, *ApJ*, 803, 102,  
doi: [10.1088/0004-637X/803/2/102](https://doi.org/10.1088/0004-637X/803/2/102)
- Edge, A., Sutherland, W., Kuijken, K., et al. 2013, *The Messenger*, 154, 32
- Faherty, J. K., Burgasser, A. J., Walter, F. M., et al. 2012, *ApJ*, 752, 56,  
doi: [10.1088/0004-637X/752/1/56](https://doi.org/10.1088/0004-637X/752/1/56)
- Faherty, J. K., Goodman, S., Caselden, D., et al. 2020, *ApJ*, 889, 176,  
doi: [10.3847/1538-4357/ab5303](https://doi.org/10.3847/1538-4357/ab5303)
- Gagné, J., Roy-Loubier, O., Faherty, J. K., Doyon, R., & Malo, L. 2018, *ApJ*, 860, 43,  
doi: [10.3847/1538-4357/aac2b8](https://doi.org/10.3847/1538-4357/aac2b8)
- Gaia Collaboration, Brown, A. G. A., Vallenari, A., et al. 2018, *A&A*, 616, A1,  
doi: [10.1051/0004-6361/201833051](https://doi.org/10.1051/0004-6361/201833051)
- Geballe, T. R., Saumon, D., Leggett, S. K., et al. 2001, *ApJ*, 556, 373, doi: [10.1086/321575](https://doi.org/10.1086/321575)
- Gelino, C. R., Kirkpatrick, J. D., Cushing, M. C., et al. 2011, *AJ*, 142, 57,  
doi: [10.1088/0004-6256/142/2/57](https://doi.org/10.1088/0004-6256/142/2/57)
- Goldman, B., Marsat, S., Henning, T., Clemens, C., & Greiner, J. 2010, *MNRAS*, 405, 1140,  
doi: [10.1111/j.1365-2966.2010.16524.x](https://doi.org/10.1111/j.1365-2966.2010.16524.x)
- Golimowski, D. A., Leggett, S. K., Marley, M. S., et al. 2004, *AJ*, 127, 3516, doi: [10.1086/420709](https://doi.org/10.1086/420709)
- Greco, J. J., Schneider, A. C., Cushing, M. C., Kirkpatrick, J. D., & Burgasser, A. J. 2019, *AJ*, 158, 182, doi: [10.3847/1538-3881/ab3ebe](https://doi.org/10.3847/1538-3881/ab3ebe)
- Griffith, R. L., Kirkpatrick, J. D., Eisenhardt, P. R. M., et al. 2012, *AJ*, 144, 148,  
doi: [10.1088/0004-6256/144/5/148](https://doi.org/10.1088/0004-6256/144/5/148)
- Haywood, M., Di Matteo, P., Lehnert, M. D., Katz, D., & Gómez, A. 2013, *A&A*, 560, A109,  
doi: [10.1051/0004-6361/201321397](https://doi.org/10.1051/0004-6361/201321397)
- Hinkel, N. R., Timmes, F. X., Young, P. A., Pagano, M. D., & Turnbull, M. C. 2014, *AJ*, 148, 54, doi: [10.1088/0004-6256/148/3/54](https://doi.org/10.1088/0004-6256/148/3/54)
- Karalidi, T., Marley, M., Fortney, J. J., et al. 2021, *ApJ*, 923, 269,  
doi: [10.3847/1538-4357/ac3140](https://doi.org/10.3847/1538-4357/ac3140)
- Kirkpatrick, J. D., Cushing, M. C., Gelino, C. R., et al. 2013, *ApJ*, 776, 128,  
doi: [10.1088/0004-637X/776/2/128](https://doi.org/10.1088/0004-637X/776/2/128)
- . 2011, *ApJS*, 197, 19,  
doi: [10.1088/0067-0049/197/2/19](https://doi.org/10.1088/0067-0049/197/2/19)
- Kirkpatrick, J. D., Gelino, C. R., Cushing, M. C., et al. 2012, *ApJ*, 753, 156,  
doi: [10.1088/0004-637X/753/2/156](https://doi.org/10.1088/0004-637X/753/2/156)
- Kirkpatrick, J. D., Martin, E. C., Smart, R. L., et al. 2019, *ApJS*, 240, 19,  
doi: [10.3847/1538-4365/aaf6af](https://doi.org/10.3847/1538-4365/aaf6af)
- Kirkpatrick, J. D., Gelino, C. R., Faherty, J. K., et al. 2021a, *ApJS*, 253, 7,  
doi: [10.3847/1538-4365/abd107](https://doi.org/10.3847/1538-4365/abd107)
- Kirkpatrick, J. D., Marocco, F., Caselden, D., et al. 2021b, *ApJL*, 915, L6,  
doi: [10.3847/2041-8213/ac0437](https://doi.org/10.3847/2041-8213/ac0437)
- Knapp, G. R., Leggett, S. K., Fan, X., et al. 2004, *AJ*, 127, 3553, doi: [10.1086/420707](https://doi.org/10.1086/420707)
- Kota, T., Kirkpatrick, J. D., Caselden, D., et al. 2022, *AJ*, 163, 116,  
doi: [10.3847/1538-3881/ac4713](https://doi.org/10.3847/1538-3881/ac4713)
- Kothari, H., Cushing, M. C., Burningham, B., et al. 2024, *ApJ*, 971, 121,  
doi: [10.3847/1538-4357/ad583b](https://doi.org/10.3847/1538-4357/ad583b)
- Lacy, B., & Burrows, A. 2023, *ApJ*, 950, 8,  
doi: [10.3847/1538-4357/acc8cb](https://doi.org/10.3847/1538-4357/acc8cb)
- Lawrence, A., Warren, S. J., Almaini, O., et al. 2007, *MNRAS*, 379, 1599,  
doi: [10.1111/j.1365-2966.2007.12040.x](https://doi.org/10.1111/j.1365-2966.2007.12040.x)
- Leggett, S. K., Liu, M. C., Dupuy, T. J., et al. 2014, *ApJ*, 780, 62,  
doi: [10.1088/0004-637X/780/1/62](https://doi.org/10.1088/0004-637X/780/1/62)



- Leggett, S. K., Morley, C. V., Marley, M. S., & Saumon, D. 2015, *ApJ*, 799, 37, doi: [10.1088/0004-637X/799/1/37](https://doi.org/10.1088/0004-637X/799/1/37)
- Leggett, S. K., Morley, C. V., Marley, M. S., et al. 2013, *ApJ*, 763, 130, doi: [10.1088/0004-637X/763/2/130](https://doi.org/10.1088/0004-637X/763/2/130)
- Leggett, S. K., Saumon, D., Marley, M. S., et al. 2007, *ApJ*, 655, 1079, doi: [10.1086/510014](https://doi.org/10.1086/510014)
- Leggett, S. K., & Tremblin, P. 2023, *ApJ*, 959, 86, doi: [10.3847/1538-4357/acfdad](https://doi.org/10.3847/1538-4357/acfdad)
- . 2024, *Research Notes of the American Astronomical Society*, 8, 13, doi: [10.3847/2515-5172/ad1b61](https://doi.org/10.3847/2515-5172/ad1b61)
- Leggett, S. K., Tremblin, P., Esplin, T. L., Luhman, K. L., & Morley, C. V. 2017, *ApJ*, 842, 118, doi: [10.3847/1538-4357/aa6fb5](https://doi.org/10.3847/1538-4357/aa6fb5)
- Leggett, S. K., Golimowski, D. A., Fan, X., et al. 2002, *ApJ*, 564, 452, doi: [10.1086/324037](https://doi.org/10.1086/324037)
- Leggett, S. K., Cushing, M. C., Saumon, D., et al. 2009, *ApJ*, 695, 1517, doi: [10.1088/0004-637X/695/2/1517](https://doi.org/10.1088/0004-637X/695/2/1517)
- Leggett, S. K., Burningham, B., Saumon, D., et al. 2010, *ApJ*, 710, 1627, doi: [10.1088/0004-637X/710/2/1627](https://doi.org/10.1088/0004-637X/710/2/1627)
- Leggett, S. K., Saumon, D., Marley, M. S., et al. 2012, *ApJ*, 748, 74, doi: [10.1088/0004-637X/748/2/74](https://doi.org/10.1088/0004-637X/748/2/74)
- Leggett, S. K., Dupuy, T. J., Morley, C. V., et al. 2019, *ApJ*, 882, 117, doi: [10.3847/1538-4357/ab3393](https://doi.org/10.3847/1538-4357/ab3393)
- Leggett, S. K., Tremblin, P., Phillips, M. W., et al. 2021, *ApJ*, 918, 11, doi: [10.3847/1538-4357/ac0cfe](https://doi.org/10.3847/1538-4357/ac0cfe)
- Lew, B. W. P., Roellig, T., Batalha, N. E., et al. 2024, *AJ*, 167, 237, doi: [10.3847/1538-3881/ad3425](https://doi.org/10.3847/1538-3881/ad3425)
- Line, M. R., Fortney, J. J., Marley, M. S., & Sorahana, S. 2014, *ApJ*, 793, 33, doi: [10.1088/0004-637X/793/1/33](https://doi.org/10.1088/0004-637X/793/1/33)
- Liu, M. C., Dupuy, T. J., Bowler, B. P., Leggett, S. K., & Best, W. M. J. 2012, *ApJ*, 758, 57, doi: [10.1088/0004-637X/758/1/57](https://doi.org/10.1088/0004-637X/758/1/57)
- Liu, M. C., Leggett, S. K., & Chiu, K. 2007, *ApJ*, 660, 1507, doi: [10.1086/512662](https://doi.org/10.1086/512662)
- Liu, M. C., Delorme, P., Dupuy, T. J., et al. 2011, *ApJ*, 740, 108, doi: [10.1088/0004-637X/740/2/108](https://doi.org/10.1088/0004-637X/740/2/108)
- Lodders, K. 1999, *ApJ*, 519, 793, doi: [10.1086/307387](https://doi.org/10.1086/307387)
- Lodieu, N., Burningham, B., Hambly, N. C., & Pinfield, D. J. 2009, *MNRAS*, 397, 258, doi: [10.1111/j.1365-2966.2008.14384.x](https://doi.org/10.1111/j.1365-2966.2008.14384.x)
- Lodieu, N., Zapatero Osorio, M. R., Martín, E. L., Rebolo López, R., & Gauza, B. 2022, *A&A*, 663, A84, doi: [10.1051/0004-6361/202243516](https://doi.org/10.1051/0004-6361/202243516)
- Lodieu, N., Pinfield, D. J., Leggett, S. K., et al. 2007, *MNRAS*, 379, 1423, doi: [10.1111/j.1365-2966.2007.12023.x](https://doi.org/10.1111/j.1365-2966.2007.12023.x)
- Lodieu, N., Burningham, B., Day-Jones, A., et al. 2012, *A&A*, 548, A53, doi: [10.1051/0004-6361/201220182](https://doi.org/10.1051/0004-6361/201220182)
- Looper, D. L., Kirkpatrick, J. D., & Burgasser, A. J. 2007, *AJ*, 134, 1162, doi: [10.1086/520645](https://doi.org/10.1086/520645)
- Lucas, P. W., Tinney, C. G., Burningham, B., et al. 2010, *MNRAS*, 408, L56, doi: [10.1111/j.1745-3933.2010.00927.x](https://doi.org/10.1111/j.1745-3933.2010.00927.x)
- Luhman, K. L. 2014, *ApJL*, 786, L18, doi: [10.1088/2041-8205/786/2/L18](https://doi.org/10.1088/2041-8205/786/2/L18)
- Luhman, K. L., Burgasser, A. J., & Bochanski, J. J. 2011, *ApJL*, 730, L9, doi: [10.1088/2041-8205/730/1/L9](https://doi.org/10.1088/2041-8205/730/1/L9)
- Luhman, K. L., Burgasser, A. J., Labbé, I., et al. 2012, *ApJ*, 744, 135, doi: [10.1088/0004-637X/744/2/135](https://doi.org/10.1088/0004-637X/744/2/135)
- Luhman, K. L., Tremblin, P., Alves de Oliveira, C., et al. 2024, *AJ*, 167, 5, doi: [10.3847/1538-3881/ad0b72](https://doi.org/10.3847/1538-3881/ad0b72)
- Mace, G. N., Kirkpatrick, J. D., Cushing, M. C., et al. 2013a, *ApJS*, 205, 6, doi: [10.1088/0067-0049/205/1/6](https://doi.org/10.1088/0067-0049/205/1/6)
- . 2013b, *ApJ*, 777, 36, doi: [10.1088/0004-637X/777/1/36](https://doi.org/10.1088/0004-637X/777/1/36)
- Mainzer, A., Cushing, M. C., Skrutskie, M., et al. 2011, *ApJ*, 726, 30, doi: [10.1088/0004-637X/726/1/30](https://doi.org/10.1088/0004-637X/726/1/30)
- Mainzer, A. K., Masiero, J. R., Abell, P. A., et al. 2023, *PSJ*, 4, 224, doi: [10.3847/PSJ/ad0468](https://doi.org/10.3847/PSJ/ad0468)
- Manjavacas, E., Goldman, B., Reffert, S., & Henning, T. 2013, *A&A*, 560, A52, doi: [10.1051/0004-6361/201321720](https://doi.org/10.1051/0004-6361/201321720)
- Marley, M. S., Saumon, D., Visscher, C., et al. 2021, *ApJ*, 920, 85, doi: [10.3847/1538-4357/ac141d](https://doi.org/10.3847/1538-4357/ac141d)
- Marocco, F., Smart, R. L., Jones, H. R. A., et al. 2010, *A&A*, 524, A38, doi: [10.1051/0004-6361/201015394](https://doi.org/10.1051/0004-6361/201015394)
- Marocco, F., Kirkpatrick, J. D., Meisner, A. M., et al. 2020, *ApJL*, 888, L19, doi: [10.3847/2041-8213/ab6201](https://doi.org/10.3847/2041-8213/ab6201)

- Martin, E. C., Kirkpatrick, J. D., Beichman, C. A., et al. 2018, *ApJ*, 867, 109, doi: [10.3847/1538-4357/aae1af](https://doi.org/10.3847/1538-4357/aae1af)
- Meisner, A. M., Leggett, S. K., Logsdon, S. E., et al. 2023, *AJ*, 166, 57, doi: [10.3847/1538-3881/acdb68](https://doi.org/10.3847/1538-3881/acdb68)
- Meisner, A. M., Caselden, D., Kirkpatrick, J. D., et al. 2020a, *ApJ*, 889, 74, doi: [10.3847/1538-4357/ab6215](https://doi.org/10.3847/1538-4357/ab6215)
- Meisner, A. M., Faherty, J. K., Kirkpatrick, J. D., et al. 2020b, *ApJ*, 899, 123, doi: [10.3847/1538-4357/aba633](https://doi.org/10.3847/1538-4357/aba633)
- Meisner, A. M., Schneider, A. C., Burgasser, A. J., et al. 2021, *ApJ*, 915, 120, doi: [10.3847/1538-4357/ac013c](https://doi.org/10.3847/1538-4357/ac013c)
- Meisner, A. M., Leggett, S. K., Logsdon, S. E., et al. 2024, *Research Notes of the American Astronomical Society*, 8, 239, doi: [10.3847/2515-5172/ad7d0e](https://doi.org/10.3847/2515-5172/ad7d0e)
- Mollière, P., Wardenier, J. P., van Boekel, R., et al. 2019, *A&A*, 627, A67, doi: [10.1051/0004-6361/201935470](https://doi.org/10.1051/0004-6361/201935470)
- Morley, C. V., Fortney, J. J., Marley, M. S., et al. 2012, *ApJ*, 756, 172, doi: [10.1088/0004-637X/756/2/172](https://doi.org/10.1088/0004-637X/756/2/172)
- Morley, C. V., Marley, M. S., Fortney, J. J., et al. 2014, *ApJ*, 787, 78, doi: [10.1088/0004-637X/787/1/78](https://doi.org/10.1088/0004-637X/787/1/78)
- Mukherjee, S., Fortney, J. J., Batalha, N. E., et al. 2022, *ApJ*, 938, 107, doi: [10.3847/1538-4357/ac8dfb](https://doi.org/10.3847/1538-4357/ac8dfb)
- Murray, D. N., Burningham, B., Jones, H. R. A., et al. 2011, *MNRAS*, 414, 575, doi: [10.1111/j.1365-2966.2011.18424.x](https://doi.org/10.1111/j.1365-2966.2011.18424.x)
- Noll, K. S., Geballe, T. R., & Marley, M. S. 1997, *ApJL*, 489, L87, doi: [10.1086/310954](https://doi.org/10.1086/310954)
- Nordström, B., Mayor, M., Andersen, J., et al. 2004, *A&A*, 418, 989, doi: [10.1051/0004-6361:20035959](https://doi.org/10.1051/0004-6361:20035959)
- Ormel, C. W., & Min, M. 2019, *A&A*, 622, A121, doi: [10.1051/0004-6361/201833678](https://doi.org/10.1051/0004-6361/201833678)
- Patten, B. M., Stauffer, J. R., Burrows, A., et al. 2006, *ApJ*, 651, 502, doi: [10.1086/507264](https://doi.org/10.1086/507264)
- Phillips, M. W., Tremblin, P., Baraffe, I., et al. 2020, *A&A*, 637, A38, doi: [10.1051/0004-6361/201937381](https://doi.org/10.1051/0004-6361/201937381)
- Pinfield, D. J., Burningham, B., Tamura, M., et al. 2008, *MNRAS*, 390, 304, doi: [10.1111/j.1365-2966.2008.13729.x](https://doi.org/10.1111/j.1365-2966.2008.13729.x)
- Pinfield, D. J., Burningham, B., Lodieu, N., et al. 2012, *MNRAS*, 422, 1922, doi: [10.1111/j.1365-2966.2012.20549.x](https://doi.org/10.1111/j.1365-2966.2012.20549.x)
- Pinfield, D. J., Gomes, J., Day-Jones, A. C., et al. 2014a, *MNRAS*, 437, 1009, doi: [10.1093/mnras/stt1437](https://doi.org/10.1093/mnras/stt1437)
- Pinfield, D. J., Gromadzki, M., Leggett, S. K., et al. 2014b, *MNRAS*, 444, 1931, doi: [10.1093/mnras/stu1540](https://doi.org/10.1093/mnras/stu1540)
- Polyansky, O. L., Kyuberis, A. A., Zobov, N. F., et al. 2018, *MNRAS*, 480, 2597, doi: [10.1093/mnras/sty1877](https://doi.org/10.1093/mnras/sty1877)
- Robbins, G., Meisner, A. M., Schneider, A. C., et al. 2023, *ApJ*, 958, 94, doi: [10.3847/1538-4357/ad0043](https://doi.org/10.3847/1538-4357/ad0043)
- Rojas-Ayala, B., Covey, K. R., Muirhead, P. S., & Lloyd, J. P. 2012, *ApJ*, 748, 93, doi: [10.1088/0004-637X/748/2/93](https://doi.org/10.1088/0004-637X/748/2/93)
- Rothermich, A., Faherty, J. K., Bardalez-Gagliuffi, D., et al. 2024, *AJ*, 167, 253, doi: [10.3847/1538-3881/ad324e](https://doi.org/10.3847/1538-3881/ad324e)
- Saumon, D., & Marley, M. S. 2008, *ApJ*, 689, 1327, doi: [10.1086/592734](https://doi.org/10.1086/592734)
- Saumon, D., Marley, M. S., Abel, M., Frommhold, L., & Freedman, R. S. 2012, *ApJ*, 750, 74, doi: [10.1088/0004-637X/750/1/74](https://doi.org/10.1088/0004-637X/750/1/74)
- Saumon, D., Marley, M. S., Cushing, M. C., et al. 2006, *ApJ*, 647, 552, doi: [10.1086/505419](https://doi.org/10.1086/505419)
- Schneider, A. C., Cushing, M. C., Kirkpatrick, J. D., et al. 2015, *ApJ*, 804, 92, doi: [10.1088/0004-637X/804/2/92](https://doi.org/10.1088/0004-637X/804/2/92)
- Schneider, A. C., Burgasser, A. J., Gerasimov, R., et al. 2020, *ApJ*, 898, 77, doi: [10.3847/1538-4357/ab9a40](https://doi.org/10.3847/1538-4357/ab9a40)
- Schneider, A. C., Meisner, A. M., Gagné, J., et al. 2021, *ApJ*, 921, 140, doi: [10.3847/1538-4357/ac1c75](https://doi.org/10.3847/1538-4357/ac1c75)
- Scholz, R. D. 2010a, *A&A*, 510, L8, doi: [10.1051/0004-6361/201014078](https://doi.org/10.1051/0004-6361/201014078)
- . 2010b, *A&A*, 515, A92, doi: [10.1051/0004-6361/201014264](https://doi.org/10.1051/0004-6361/201014264)
- Scholz, R. D., Bihain, G., Schnurr, O., & Storm, J. 2011, *A&A*, 532, L5, doi: [10.1051/0004-6361/201117297](https://doi.org/10.1051/0004-6361/201117297)
- . 2012, *A&A*, 541, A163, doi: [10.1051/0004-6361/201218947](https://doi.org/10.1051/0004-6361/201218947)
- Skrutskie, M. F., Cutri, R. M., Stiening, R., et al. 2006, *AJ*, 131, 1163, doi: [10.1086/498708](https://doi.org/10.1086/498708)

- Smart, R. L., Jones, H. R. A., Lattanzi, M. G., et al. 2010, *A&A*, 511, A30, doi: [10.1051/0004-6361/200913633](https://doi.org/10.1051/0004-6361/200913633)
- Strauss, M. A., Fan, X., Gunn, J. E., et al. 1999, *ApJL*, 522, L61, doi: [10.1086/312218](https://doi.org/10.1086/312218)
- Subasavage, J. P., Jao, W.-C., Henry, T. J., et al. 2009, *AJ*, 137, 4547, doi: [10.1088/0004-6256/137/6/4547](https://doi.org/10.1088/0004-6256/137/6/4547)
- Sutherland, W., Emerson, J., Dalton, G., et al. 2015, *A&A*, 575, A25, doi: [10.1051/0004-6361/201424973](https://doi.org/10.1051/0004-6361/201424973)
- Tan, X., & Showman, A. P. 2021, *MNRAS*, 502, 678, doi: [10.1093/mnras/stab060](https://doi.org/10.1093/mnras/stab060)
- Tannock, M. E., Metchev, S., Heinze, A., et al. 2021, arXiv e-prints, arXiv:2103.01990. <https://arxiv.org/abs/2103.01990>
- Thompson, M. A., Kirkpatrick, J. D., Mace, G. N., et al. 2013, *PASP*, 125, 809, doi: [10.1086/671426](https://doi.org/10.1086/671426)
- Tinney, C. G., Burgasser, A. J., & Kirkpatrick, J. D. 2003, *AJ*, 126, 975, doi: [10.1086/376481](https://doi.org/10.1086/376481)
- Tinney, C. G., Burgasser, A. J., Kirkpatrick, J. D., & McElwain, M. W. 2005, *AJ*, 130, 2326, doi: [10.1086/491734](https://doi.org/10.1086/491734)
- Tinney, C. G., Faherty, J. K., Kirkpatrick, J. D., et al. 2014, *ApJ*, 796, 39, doi: [10.1088/0004-637X/796/1/39](https://doi.org/10.1088/0004-637X/796/1/39)
- . 2012, *ApJ*, 759, 60, doi: [10.1088/0004-637X/759/1/60](https://doi.org/10.1088/0004-637X/759/1/60)
- Tinney, C. G., Kirkpatrick, J. D., Faherty, J. K., et al. 2018, *ApJS*, 236, 28, doi: [10.3847/1538-4365/aabad3](https://doi.org/10.3847/1538-4365/aabad3)
- Tremblin, P., Padiou, T., Phillips, M. W., et al. 2019, *ApJ*, 876, 144, doi: [10.3847/1538-4357/ab05db](https://doi.org/10.3847/1538-4357/ab05db)
- Tsvetanov, Z. I., Golimowski, D. A., Zheng, W., et al. 2000, *ApJL*, 531, L61, doi: [10.1086/312515](https://doi.org/10.1086/312515)
- Tu, Z., Wang, S., & Liu, J. 2024, arXiv e-prints, arXiv:2409.19191, doi: [10.48550/arXiv.2409.19191](https://doi.org/10.48550/arXiv.2409.19191)
- Visscher, C., Lodders, K., & Fegley, Bruce, J. 2006, *ApJ*, 648, 1181, doi: [10.1086/506245](https://doi.org/10.1086/506245)
- Vrba, F. J., Henden, A. A., Luginbuhl, C. B., et al. 2004, *AJ*, 127, 2948, doi: [10.1086/383554](https://doi.org/10.1086/383554)
- Warren, S. J., Mortlock, D. J., Leggett, S. K., et al. 2007, *MNRAS*, 381, 1400, doi: [10.1111/j.1365-2966.2007.12348.x](https://doi.org/10.1111/j.1365-2966.2007.12348.x)
- Wright, E. L., Eisenhardt, P. R. M., Mainzer, A. K., et al. 2010, *AJ*, 140, 1868, doi: [10.1088/0004-6256/140/6/1868](https://doi.org/10.1088/0004-6256/140/6/1868)
- Wright, E. L., Skrutskie, M. F., Kirkpatrick, J. D., et al. 2013, *AJ*, 145, 84, doi: [10.1088/0004-6256/145/3/84](https://doi.org/10.1088/0004-6256/145/3/84)
- Yurchenko, S. N., & Tennyson, J. 2014, *MNRAS*, 440, 1649, doi: [10.1093/mnras/stu326](https://doi.org/10.1093/mnras/stu326)
- Zahnle, K. J., & Marley, M. S. 2014, *ApJ*, 797, 41, doi: [10.1088/0004-637X/797/1/41](https://doi.org/10.1088/0004-637X/797/1/41)
- Zalesky, J. A., Saboi, K., Line, M. R., et al. 2022, *ApJ*, 936, 44, doi: [10.3847/1538-4357/ac786c](https://doi.org/10.3847/1538-4357/ac786c)
- Zapatero Osorio, M. R., Martín, E. L., Bouy, H., et al. 2006, *ApJ*, 647, 1405, doi: [10.1086/505484](https://doi.org/10.1086/505484)
- Zhang, Z., Liu, M. C., Claytor, Z. R., et al. 2021, *ApJL*, 916, L11, doi: [10.3847/2041-8213/ac1123](https://doi.org/10.3847/2041-8213/ac1123)
- Zhang, Z., Liu, M. C., Marley, M. S., Line, M. R., & Best, W. M. J. 2021, *ApJ*, 921, 95, doi: [10.3847/1538-4357/ac0af7](https://doi.org/10.3847/1538-4357/ac0af7)
- Zhang, Z. H., Burgasser, A. J., Gálvez-Ortiz, M. C., et al. 2019, *MNRAS*, 486, 1260, doi: [10.1093/mnras/stz777](https://doi.org/10.1093/mnras/stz777)